THE STRUCTURE AND AGING OF MARTENSITE

by

ANDREW MICHAEL SHERMAN

S.B., Massachusetts Institute of Technology
(1967)

Submitted in partial fulfillment of the requirements

for the degree of

DOCTOR OF PHILOSOPHY

at the

Massachusetts Institute of Technology

September, 1972

Signature of Author _____
Department of Metallurgy and
Materials Science, August 14, 1972

Certified by_____
Thesis Supervisor

Accepted by_____
Chairman, Departmental Committee on Graduate
Students

ABSTRACT

THE STRUCTURE AND AGING OF MARTENSITE

by

ANDREW MICHAEL SHERMAN

Submitted to the Department of Metallurgy and Materials Science on August 14, 1972 in partial fulfillment of the requirements for the degree of Doctor of Philosophy.

The structure and aging of virgin lath and twinned martensites were investigated by means of X-ray diffraction, transmission electron microscopy, and electrical resistivity measurements. Seventeen iron-nickel-carbon alloys with 18, 21 and 24 weight percent nickel and carbon contents from zero up to 0.62 weight percent were chosen to provide martensites of both morphologies.

The lath martensite consisted of packets of highly dislocated laths, while the twinned martensite took the form of internally twinned acicular plates, with the {112} twins spaced 60 to 100 angstroms apart. The virgin twinned martensite is found to be body-centered tetragonal with the axial ratio proportional to the carbon content. There is indirect evidence that virgin lath martensite is also tetragonal. Interstitial ordering theories are shown to be invalid in accounting for the tetragonality of virgin martensite. No indication of carbon disordering during or after martensite formation was noted.

The aging of both martensitic morphologies proceeds in four steps, depending on the temperature of aging. The first is a dislocation relaxation, which is detectable only in specimens aged below room temperature; the associated activation energy is about 3 kcal per mole. Secondly, carbon-rich clusters form in the martensite at temperatures above $-30°C$, the activation energy being approximately 21 kcal per mole;

this suggests that carbon diffusion is the rate-controlling process. The third step, occurring above 100°C, is the formation of ε-carbide. There is some indication that the carbide forms directly from the clusters; the corresponding activation energy of 35 kcal per mole suggests that the rate-controlling process may be the pipe-diffusion of iron atoms away from growing carbide particles. The fourth step in the sequence is the precipitation of cementite at temperatures above 200°C; here, the activation energy is the same as that for ε-carbide formation. Recovery and recrystallization follow the latter stage. No significant differences in aging behavior between the lath and twinned martensites were observed, indicating that the substructure does not play a major role in the aging phenomena.

Thesis Supervisor: Morris Cohen

            Title: Ford Professor of Materials
                    Science and Engineering

TABLE OF CONTENTS

LIST OF FIGURES

LIST OF TABLES

ACKNOWLEDGEMENTS

It would have been impossible to carry out a research project such as this thesis without the help of many people who were willing to share their knowledge, experience, facilities and time. The author feels deeply indebted to:

Professor Morris Cohen, his thesis advisor, for the ideas, encouragement and guidance he was always prepared to provide.

Professor John Vander Sande for help with electron microscopy.

Professor Roy Kaplow for many helpful discussions.

Mr. Edwin Alexander, Mr. Charles Bir, Mr. Walter Fitzgerald, Mr. Arthur Gregor, Mr. Peter Kelleher, Mr. Robert Kelley, Mrs. Kathrine Landry, and Mr. Anthony Santangelo for help with various phases of the experiments.

Miss Marguerite Meyer, Mrs. Jane Operacz, and Mrs. Miriam Yoffa Rich, who provided support, advice and help in many, many ways.

Fellow students James Baker, Subir Bhattacharyya, Joel Clark, George Eldis, Fred Fletcher, and James Pugh whose help and friendship were invaluable.

The author extends his deepest thanks to the Climax Molybdenum Company of Michigan, for financial support in the form of a fellowship.

The author also wishes to thank the United States Steel Company Research Center for preparing the alloys.

Chapter I

INTRODUCTION

Steels had been used for several thousand years before anything was known about why their properties could be changed by the application of thermal and mechanical treatments. (1) In the early part of this century, it was realized that the large increase in the strength of steel upon quenching from high temperatures is due to a transition in structure from austenite, a face-centered cubic phase, to martensite, a body-centered structure. (2) Further changes in mechanical properties upon reheating the quenched steel were explained by the discovery of a series of structures, resulting from such tempering treatments. (3-4)

Since these structures were first observed there has been substantial research activity aimed at a better description of the structures and how, when, and why they form. With the advent of more modern research techniques, such as transmission electron microscopy and Mössbauer measurements, more details of martensite formation and aging have been studied. This research is meant to provide a still more complete description of the structure of martensite and the decomposition products formed during aging.

Chapter II

LITERATURE REVIEW

2.1 Martensite Formation

Martensite is the name given to the phase produced by
a diffusionless shear transformation. In iron alloys, such
transformations take place when the face-centered cubic
austenite is cooled sufficiently rapidly to avoid the
competing isothermal reactions. The martensitic transform-
ation begins when the temperature of the steel is cooled
below M_s, the martensite start temperature, and it proceeds
at speeds approaching that of sound in the metal. (5) Models
to account for the kinetic features of the nucleation and
growth of martensite have been developed by Kaufman and
Cohen (6), Clapp (7), and others. A recent review of the
subject was given by Kaufman. (8)

Crystallographic theories of the martensitic trans-
formation have been developed on the basis of a phenomenological
approach to the question of how the transformation from
austenite to martensite is accomplished. A review of such
theories was given by Dunne and Wayman. (9) The
phenomenological description of the martensitic transformation
is given by the matrix relationship:

$$P_1 = RBP \qquad\qquad (1)$$

in which P_1 is the shape strain of the transformation,
which is composed of three parts: R, the orientation
relationship between the parent austenite and the martensite,
B, the Bain strain, and P, an inhomogeneous shear in the
martensite which accomodates the martensite to the austenite.

The cumulative effect is to produce an invariant-plane transformation.

2.1.1 Martensite Morphology

Two distinct morphologies of martensite have been observed. (10-15) One forms in alloys with relatively high M_s temperatures and consists of packets of laths, with a high dislocation density. The other morphology forms in alloys with lower M_s temperatures and consists of acicular plates with an internal structure of very fine twins about 60 to 100Å apart. The dislocation density of this type appears to be much lower than that of the first type. Because of the shape of the acicular plates, it is usual for much more retained austenite to be present with the twinned morphology than with the lath.* Figures 1 and 2 are optical and transmission electron micrographs of the two morphologies.

It has been proposed (10,11,16) that the inhomogeneous shear of the martensite transformation (P in eqn. 1) can occur by slip or twinning. In lath martensite, which is formed at higher temperatures, this shear is accomplished by slip leading to the high dislocation density of the laths. Since twinned martensite forms at lower M_s temperatures, the shear is accomplished by twinning, because twinning becomes

*The terminology used in this work will be "lath martensite" to indicate the high-M_s dislocated morphology and "twinned martensite" to indicate the low-M_s acicular plate martensite.

(a) Optical micrograph 1% Nital etch. 1000X
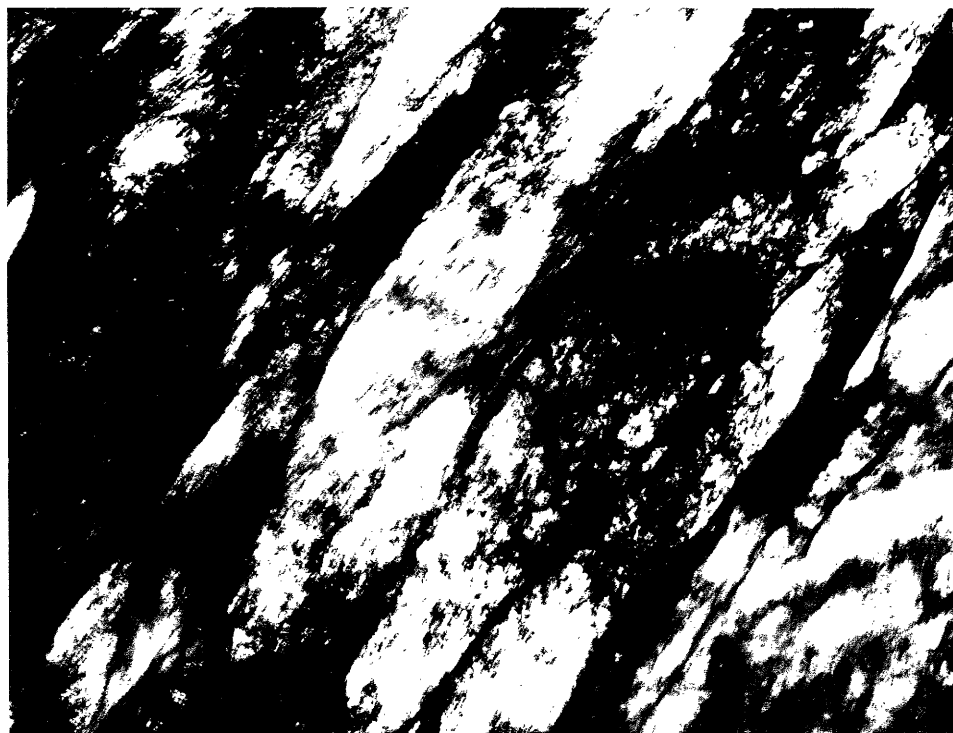
(b) Transmission electron micrograph 44000X

Figure 1: Micrographs of Lath Martensite in an 18Ni-0.11C Alloy.

(a) Optical micrograph 1% Nital etch. 1000X

(b) Transmission electron micrograph 14000X

Figure 2: Micrographs of Twinned Martensite in an 18Ni-0.4C Alloy.

relatively easier than slip at lower temperatures. Some support for this idea has come from experiments which produced changes in M_S temperature by the application of high pressure or mechanical treatments resulting in a change in martensite morphology. (16-19) Davies and Magee (20-21) have extented this line of thought to a consideration of austenite ferromagnetism as a necessary condition to the formation of twinned martensite in Fe-Ni alloys. Ferromagnetic austenites are substantially stronger than paramagnetic austenites, and hence could influence the mode of deformation by which martensite forms.

Since the morphology of martensite depends on the M_S temperature, the addition of alloying elements which change M_S can affect the morphology of the martensite. (12-13) Figure 3 shows the morphology for Fe-Ni-C alloys. There is a range of compositions for which mixed lath and twinned structures have been observed. The breadth of this range decreases in the alloys with higher nickel contents. The M_S temperature at which the lath-to-twinned change takes place is lower for alloys with larger amounts of nickel.

2.1.2 Martensite Tetragonality

Carbon occupies octahedral interstitial positions in the iron lattices of both austenite and martensite. In austenite (Fig. 4) the iron atoms forming the corners of the octahedron are equidistant from the interstitial site; hence when the site is occupied by a carbon atom the lattice is expanded symmetrically. In martensite (Fig. 5) the
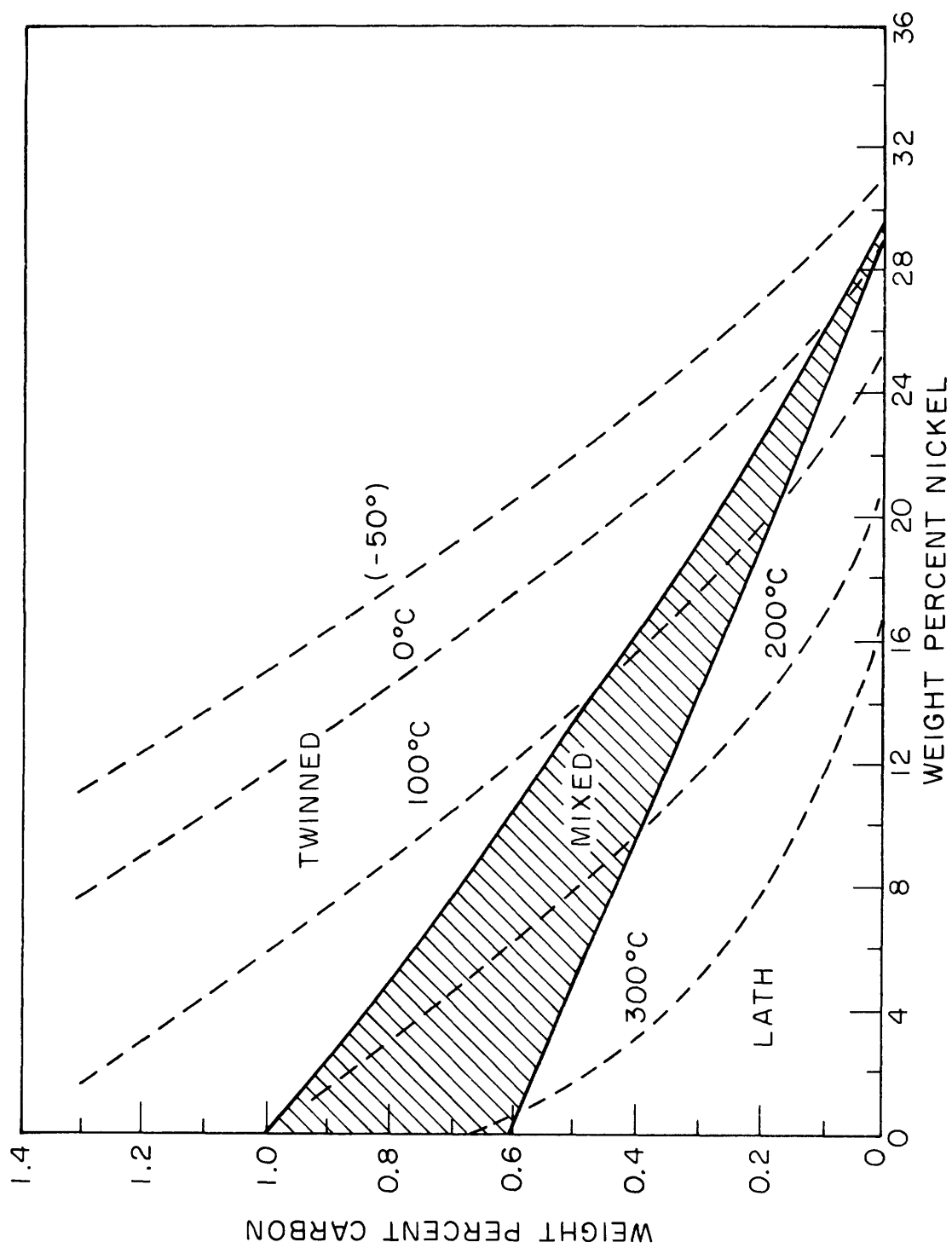
FIGURE 3.   THE MORPHOLOGY AND M_s TEMPERATURES OF Fe–Ni–C MARTENSITE
AS A FUNCTION OF COMPOSITION (AFTER WINCHELL (22))

20

Octahedral Sites ●   Iron Atoms ○
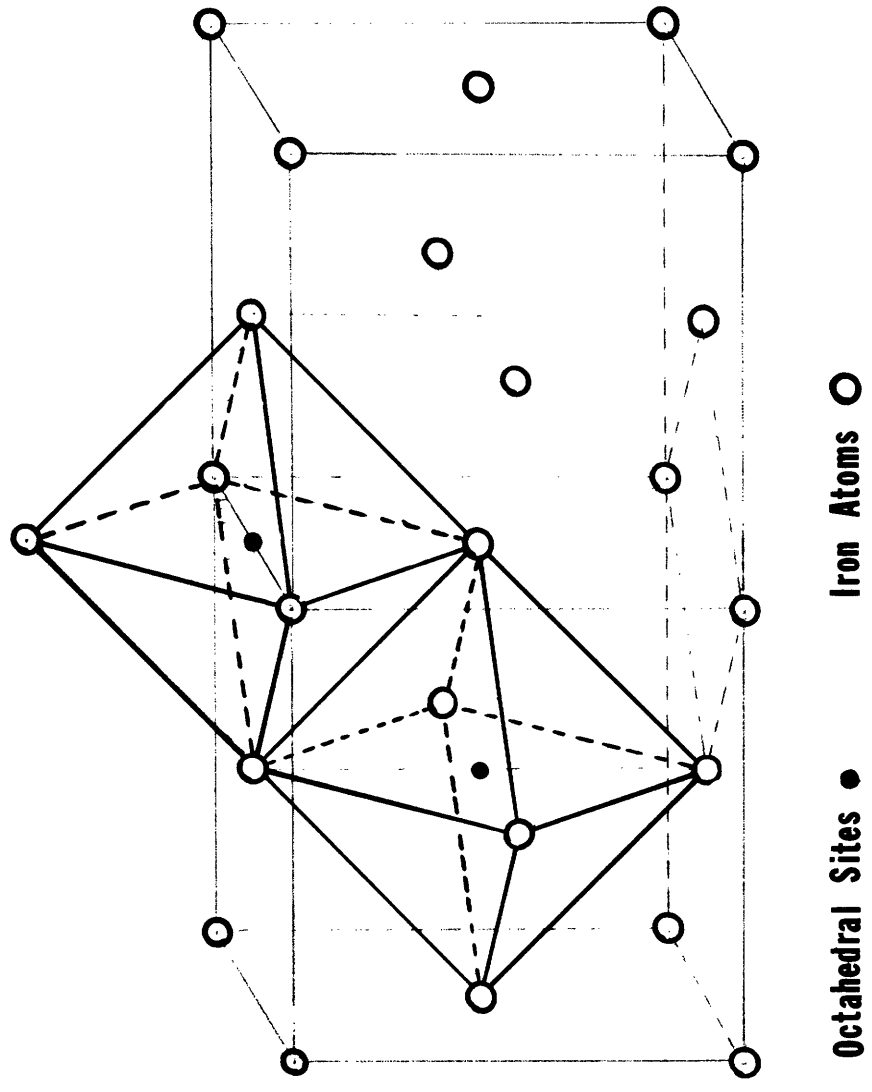
FIGURE 4.   fcc AUSTENITE LATTICE WITH POSITIONS
OF OCTAHEDRAL SITES INDICATED

21

Octahedral Sites ●   **Iron Atoms** ○
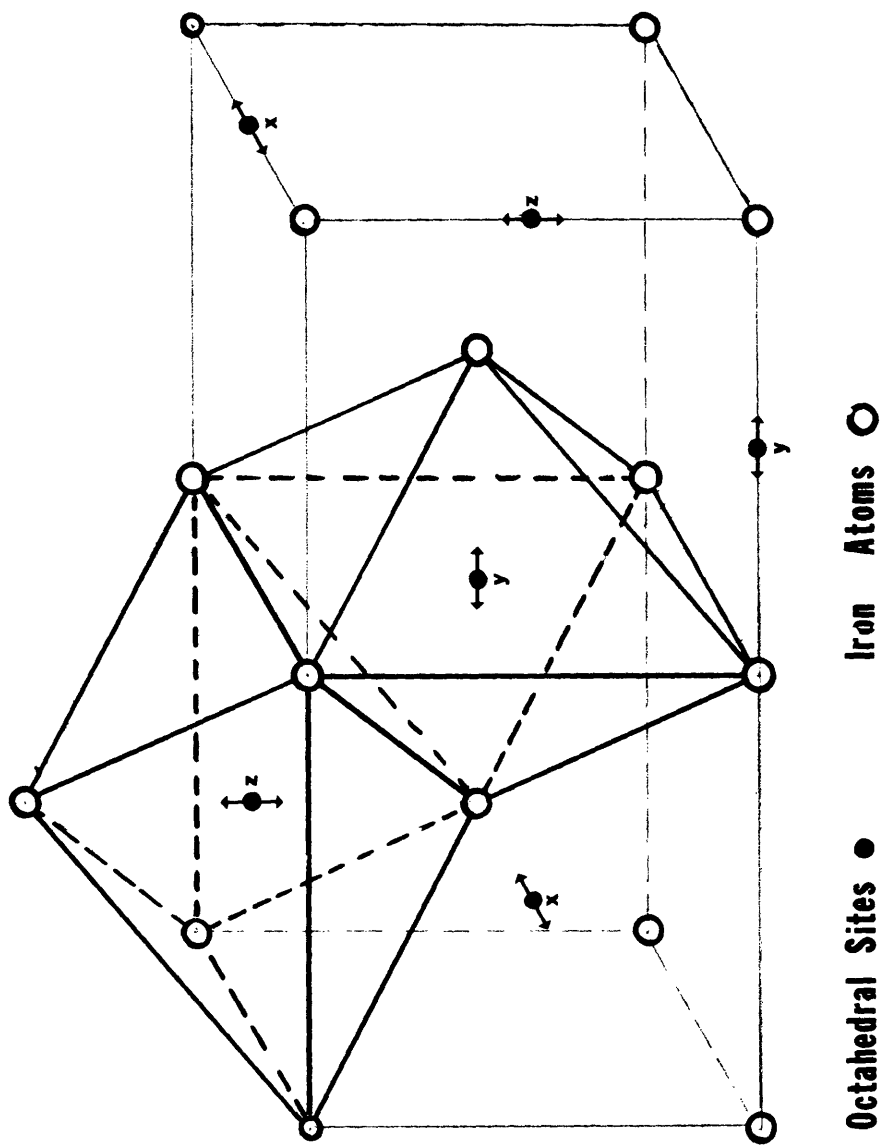
FIGURE 5. BODY-CENTERED MARTENSITE LATTICE SHOWING THE THREE SETS OF OCTAHEDRAL SITES

octahedral sites have two irons closer than the other four irons, thus forming a distorted octahedron. When such a site is occupied, the lattice distortion is asymmetrical. (23-26) There are three sets of octahedral sites in bcc iron. If only one set of sites is occupied, the asymmetric distortions will lead to expansion in one of the three {001} directions and contractions in the other two.

The Bain distortion part of martensite formation (B in eqn. 1) is the collapse of the fcc austenite lattice into the body-centered martensite lattice. Due to the nature of this distortion, if there are some carbon atoms in solution they will occupy only one of the three sets of octahedral sites. The cumulative effect of the asymmetric distortions of the occupied sites leads to the martensite being body-centered tetragonal. Winchell and Speich (27) have offered a systematic treatment of those situations in which tetragonality may be produced in martensite as a result of asymmetric point defects. There have been a number of studies (28-30) which measured this tetragonality; the c/a ratio appears to vary linearly with carbon content.

Tetragonal iron-carbon martensite can be thought of as an ordered solid solution, since it is the occupation of only one of three sets of octahedral sites which causes tetragonality. Zener and others (31-35) have proposed theories to account for the ordering of carbons to one set of sites. Although the details of each theory are different, each predicts that, for a given carbon concentration, there

is a critical temperature below which the structure can
minimize its free energy, and accomodate the anisotropic
strain due to the interstitial atoms, by allowing them to
occupy one set of octahedral sites in preference to the
other two. Thus, below this critical temperature, there
is a driving force for an ordering reaction that converts
the bcc structure to bct. The prediction for the critical
temperature for ordering is of the same order of magnitude
for all the theories, namely T_c is about 1000 times the
weight percent carbon in the alloy.

Owen, et al. (36) have suggested that such an order-
disorder reaction may be at play in the formation of bcc
martensite in alloys with low carbon contents. In such
alloys T_c is lower than M_s leading to carbon disordering
immediately on formation of the martensite. They cite as
supporting evidence some observations of bcc virgin martensite.
On the other hand, there have never been observations of
actual ordering and disordering of interstitials, thus
confirming the existence of a critical temperature. However,
this may be due to the intervention of aging effects
removing the carbons from solution before disordering
could be observed. So the question of whether interstitial
ordering reactions occur is still open. It would seem that
the structure of martensite must be tetragonal at the
moment of formation due to the inherited distribution of
carbons as a result of the Bain strain, but it is not
certain if any changes occur immediately afterward. There
is ample evidence (28-30) that twinned martensite is

tetragonal when observed in the virgin condition, but the
case of lath martensite has not been fully explored. The
lower carbon contents of alloys forming lath martensite lead
to high M_s and low T_c values, so if the ordering theories
are valid it is likely that disordering will cause lath
martensite to be cubic. Also, segregation of carbons to
dislocation sites during the quench could deplete the
lattice of interstitials and lead to the observation of
cubic martensite.

2.2 Martensite Aging

The equilibrium concentration of carbon in α-iron
below 500°C is less than 0.01 weight percent. (37) Thus
Fe-C martensite is a metastable phase, with much more than
the equilibrium amount of carbon trapped in solution due to
the diffusionless nature of the transformation. If
provided with the necessary activation energy, martensite
will undergo changes resulting in the formation of structures
closer to the equilibrium mixture of α-ferrite and
cementite (Fe_3C). These changes are thermally activated,
and those which occur at elevated temperatures are called
tempering, while the more subtle low temperature changes
have been called aging.

2.2.1 The Stages of Tempering

The tempering of steel may be divided into three
stages. (3-4) Averbach and Cohen, et al. (29,38-40) have
provided an extensive description of the structural changes
which occur due to tempering. Their results showed that the

first stage of tempering consists of the formation of

ε-carbide (41) a hexagonal close-packed structure of

approximate composition $Fe_{2.4}C$, at the same time as a low-

carbon martensite appears. From its c/a ratio the

composition of the low-carbon martensite seems to be

0.25 weight percent carbon. Its appearance is discontinuous;

that is, a second, distinct $(002)_M$ line appears on diffraction

films and its intensity increases while the intensity of the

original $(002)_M$ line decreases as tempering progresses. The

second stage of tempering involves the transformation of

retained austenite by isothermal reactions. Usually the

product of the second stage is bainite, although in some steels

this stage may not occur at all. The third stage was found

to be the precipitation of cementite, an orthorhombic

structure of composition Fe_3C. As tempering continues into

the third stage, the ε-carbide disolves and the carbon

content of the matrix drops from 0.25 weight percent to its

equilibrium value, with a concurrent loss of tetragonality.

Eventually the cementite coarsens and spherodizes, and

recovery and recrystallization also occur producing a

structure of α-ferrite and spherodized cementite. All of

the changes due to tempering are thermally activated (hence

temperature- and time-dependant) so there is usually some

overlap between the stages.

Since the time that the stages of tempering were set

forth, more details and refinements of the process have been

explored. Wells (42) showed that orientation relationships

exist between both the ε-carbide and cementite lattices and

the martensite lattice. Information about the kinetics of the various stages has been provided by a number of investigators. (29-30,38,43-44) The activation energy appears to increase during the course of tempering from initial values of about 15 kcal. per mole up to 35 kcal. per mole during stage three. It has been suggested (43-44) that tempering consists of several simultaneous or overlapping processes, each with a different activation energy. The work of Hoffman (45), Kalish and Cohen (46) and Barton (47) has questioned the idea that ε-carbide is in equilibrium with low-carbon martensite. They suggest that the substructure, particularly the dislocation density, of the martensite is a determining parameter for the appearance of ε-carbide. Recently, Hirotsu and Nagakura (48) have presented evidence that the structure of the carbide precipitated during the first stage is orthorhombic, not hcp, and call the structure η-carbide.

2.2.2 The Early Stages of Aging

Until recently most tempering experiments did not start with the martensite in its virgin state. Since the M_S temperatures of most steels are well above room temperature, changes may take place while the quenching itself is going on. This phenomena has been called autotempering. Furthermore, cooling only to room temperature is not enough to prevent all aging. Calculations by Cohen (2) have shown that the jump frequency of carbon at room temperature is great enough to allow aging changes

to occur. Speich (49) has shown that even with very
rapid cooling rates autotempering can take place. So in
order to observe virgin martensite, alloys with low M_S
temperatures must be used and the quenching must be as
rapid as possible to liquid nitrogen temperature ($-196\,°C$).
The first systematic study of virgin martensites in this
way was by Winchell and Cohen.(30) A more recent study
was done by Eldis (44), who used resistivity measurements
on specimens tempered at a range of temperatures from -95
to $300\,°C$ to obtain data on the kinetics of tempering.
Mössbauer measurements by Genin and Flinn (50) and by
Choo and Kaplow (51) have shown that carbon atoms cluster
during aging at temperatures less than $100°C$. The
formation of clusters corelates quite well with a resistivity
peak observed by Eldis in alloys tempered at similar
temperatures. Choo and Kaplow have concluded that the
clusters approach the approximate composition Fe_4C, with
an fcc structure analogous to that of Fe_4N. Izotov and
Utevskiy (52) have reached a similar conclusion on the
basis of electron diffraction data. Computer calculations
by Johnson, et al. (53-54) have predicted that there is
a binding energy between carbon-atom pairs as have several
earlier calculations. (33,55-56) Hoffman (57-58) has
calculated that a spinodal decomposition or clustering
reaction of interstitial carbons would lead to a reduction
in the elastic free energy of the martensite lattice. Thus,
it appears that there is a driving force for the formation

of clusters of carbons and that such clusters are observed at an early stage in the aging of martensite.

Besides clustering the segregation of carbons to dislocation sites has been considered as a pre-carbide phase of aging. Speich (49) has estimated that 80 percent of the carbon in low-carbon, high-M_S steels segregates to dislocations or cell boundaries as a result of autotempering, and that further segregation occurs on tempering below 150 °C before the formation of carbides. Kalish and Cohen (46) have calculated the dislocation densities required to provide enough sites for the segregation of carbons. A lath martensite whose dislocation density is of the order of 10^{11} to 10^{12} cm. per cc has enough sites to accomodate about 0.1 weight percent carbon without the precipitation of carbides. Eldis (44) included carbon segregation to dislocations as a step in the aging of martensite. He attributed a drop in resistivity after the peak to the segregation of 0.12 weight percent carbon to dislocation sites. However, if segregation to dislocations is an important factor then it may overlap with cluster formation, thus removing from the lattice some carbon atoms which otherwise would have found their way to clusters. It must also be pointed out that the dislocation densities of twinned martensites appear to be lower than those of lath martensites so carbon segregation should be less of a factor in the aging of this morphology.

In line with the idea of segregation to dislocations,

Lement and Cohen (59) have proposed that dislocation
segregation is an important part of the formation
process of ε-carbide. Furthermore, their model accounts
for the discontinuous appearance of the low-carbon
tetragonal martensite accompanying ε-carbide formation.

A review of the basic ideas of order-disorder,
clustering and segregation of carbons in martensite has
been given by Kurdjumov and Khachaturyan.(60) It is
their opinion that all of these phenomena are at play
in the formation and aging of martensite. They also
report observations of some unusual c/a ratio increases
upon aging in certain alloys.

One other phenomenon has been noted during the
very early stage of aging. Eldis (44) observed a small
but reproducible drop in resistivity in alloys tempered
as low as -95°C and taking only a few minutes. He
suggested that this may be a result of a slight
rearrangement of dislocations.

Chapter III

PURPOSE AND PLAN OF RESEARCH

In view of the fact that the structures of both
lath and twinned martensites have not been well determined,
this work sought to settle the question of the tetragon-
ality of both types in the virgin condition. Also a more
complete description of the fine structure of each was
attempted. Furthermore, it was evident that the structures
formed on aging were not well understood. It was felt
that the possibility of differences in aging behavior as a
result of the structural differences of the two martensitic
morphologies had not been fully explored. Finally, the
applicability of the ordering theories had not been tested
experimentally.

The research techniques used to approach the above
problems were x-ray diffraction, optical and electron
microscopy and electrical resistivity measurements. The
x-ray work was used to determine the crystal structure of
unaged martensite and to follow changes in that structure
as the martensite was aged. Microscopy was used to
determine the microstructure and the fine structure of
martensite at various stages of aging. The results of
Mössbauer experiments performed by others (50-51)
provided information about changes in atomic arrangements
due to aging. Resistivity measurements tied all the
structural observations together by providing kinetic data

for each change. Thus, aging changes in martensite could
be followed by several different means, which allowed a
more thorough understanding of the phenomena than could be
achieved by the use of any single method.

Chapter IV

EXPERIMENTAL PROCEDURES

4.1 Materials

Three series of Fe-Ni-C alloys were designed for
this study, and prepared by the United States Steel
Company. The series had 18, 21 and 24 weight percent
nickel, with a range of carbon contents such that some
alloys of each series would form lath martensite and the
others form twinned martensite. The nickel contents were
chosen because in such alloys the transition from lath to
twinned morphology occurs over a relatively small range of
carbon contents (Fig. 3) and because the M_S temperatures
are the lowest of any alloys forming lath martensite. The
latter was desireable to avoid autotempering. Table 1
lists the compositions and estimated M_S temperatures of
the alloys.

4.2 Alloy Processing

The alloys were received in the form of half-inch
thick hot-rolled plates. Rods 2 inches long and 0.480
inches in diameter were machined from sections of the plates.
Care was taken to remove all scale from the surfaces of the
rods. The rods were swaged to 0.241 inches in diameter with
intermediate annealings for 10 hours at 1000°C in argon
filled vycor capsules as necessary. After swaging, the
rods were given a homogenizing anneal at 1200°C for 24 hours
and furnace cooled. Following homogenization, the rods

Table 1   33

COMPOSITIONS AND ESTIMATED M_s TEMPERATURES

OF ALLOYS STUDIED

U. S. STEEL HEAT NUMBER	C(w/o)	Ni(w/o)	M_s(°C)
1399A	0.0033	18.3	250
1399B	0.11	18.1	180
1400A	0.40	18.3	20
1400B	0.50	18.3	10
1400C	0.62	18.4	-20
1401A	0.0078	20.8	200
1401B	0.10	20.8	130
1401C	0.20	20.7	80
1402A	0.25	21.8	40
1402B	0.30	21.5	25
1403A	0.0078	24.6	110
1403B	0.12	24.6	50
1403C	0.14	24.7	35
1404A	0.19	25.5	10
1404B	0.24	25.5	-10
1404C	0.28	25.2	-30

All alloys contained less than 0.003 w/o Si and less than 0.005 w/o Mn.

were centerless ground to 0.190 inches in diameter in order
to remove any scale, decarburized layer, or surface
contamination due to swaging. Sections of the rods were
swaged and wire drawn to 0.031 inches in diameter with
intermediate annealing at 850°C for 1/2 hour in a vacuum
better than 1×10^{-5} torr, as needed.

4.3 Rapid Quenching

A rapid quenching apparatus was constructed
consisting of an inconel tube inside a vertical one-inch
diameter tube furnace. The tube had an inlet and an outlet
for a continuously flowing argon atmosphere. A second,
smaller tube inside the first held the specimen in the
center of the hot zone of the furnace. This inner tube
was conected to a gas reservoir, which could be filled and
emptied by operating a pair of electrically activated valves.
The gas reservoir was pressurized with argon at 2500 pounds-
per-square-inch. When the pressure in the reservoir was
released, it forced the specimen downward through an
aluminum-foil membrane at the bottom of the tube and into
a water-quench bath. The specimen was immediately
transferred to a liquid-nitrogen bath. The time elapsed
during the entire quenching operation was less than four
seconds.

In practice the specimen was installed in the
quencher with the furnace at room temperature, and the
quencher was thoroughly purged by the flowing argon
atmosphere before the heating began. It took about 30

minutes to heat up to the 850 °C austenitizing temperature, which was held for 15 minutes before quenching.

4.4 Resistivity Measurements

Resistivity specimens were made from two-inch lengths of the 0.031 inch diameter wire by spotwelding two #24 B&S gauge pure nickel wires to each end. The diameter and length of the specimens were recorded. Then the specimens were quenched using the rapid quencher, and kept in liquid nitrogen for a minimum of one day before any resistivity measurements began. This insured that any possible isothermal transformation at liquid nitrogen temperature would have occurred before the measurements, and hence not interfere with the interpretation of the subsequent resistivity changes due to aging.

The initial resistance of each specimen was measured. The specimen was then repeatedly upquenched in an aging bath, and returned to the liquid-nitrogen bath at intervals for resistance measurements. All resistance measurements were made with the specimens at -196°C (liquid-nitrogen), with a Kelvin double bridge. The resistances could be measured with an accuracy of ±0.00001 ohms. The measured resistances were converted to resistivities by using the formula:

$$\rho = R \frac{A}{L} \qquad (2)$$

in which ρ=resistivity

R=measured resistance

A=cross sectional area of the specimen

L=test length of the specimen

The accuracy of the resistivity values was ±2 percent due to the difficulty of measuring the dimensions of the specimen, with greater than this precision. However, changes in the resistivity of a given specimen by 0.1 percent or more could be accurately measured, because in this case only the sensitivity of the Kelvin bridge is important.

Various media were used for aging baths at different temperatures, Table 2. The elevated temperature baths were heated electrically. The subambient temperatures were obtained by passing cold nitrogen gas, from a liquid-nitrogen tank, through a coil immersed in the bath. Temperature control was maintained by regulating the gas flow with a solonoid valve operated by a temperature controller. Temperature variation was ±2°C for all baths.

In this way resistivity vs. aging time curves were generated for each alloy at many different temperatures, with all measurements taken at the common temperature of -196°C.

4.5 Microscopy

Quarter-inch lengths of the 0.190-inch diameter rods were quenched using the rapid quenching apparatus. The quenched specimens were aged for one hour in the same baths as the resistivity specimens. However, only aging treatments

above room temperature were used for the microscopy, because it was impossible to prepare and examine any microscope specimens without warming them at least to room temperature. After aging the rods were cut into discs 0.015-inch thick using a water cooled carborundum cut off wheel 0.010-inch thick.

4.5.1 Optical Microscopy

A disc sample was mounted and polished in the conventional way, and then etched with one percent nital to bring out the microstructure. Some of the resistivity specimens were also prepared in the above way. Point counting was performed to determine the volume fraction of retained austenite in these specimens. A sufficient number of points were counted to insure ±10 percent accuracy of the data.

4.5.2 Electron Microscopy

The disc samples were hand-ground to 0.010-inch thicknesses using 4/0 emery paper, taking care to remove an equal amount of material from each side. The ground discs were indented electrolytically using a 25 percent nitric acid-75 percent water jet 1.5 millimeters in diameter, with the jet nozzle one centimeter above the specimen. Each side of a disc was jetted for 10 seconds at 120 volts. The indented portion of the disc was then about 0.007-inch thick. Final thinning was done by electrolytic polishing in a solution of anhydrous sodium

chromate and glacial acetic acid mixed in the ratio of one gram chromate to five milliliters acid. This operation was done in a vertical polishing set up in which the specimen was illuminated from below and viewed constantly from above through a 10 power microscope. 15 volts was applied to the well-agitated electrolytic bath. Polishing continued until a hole appeared in the specimen, usually after about 80 minutes.

After polishing the specimens were carefully washed in distilled water and air dried. Specimens were stored in an evacuated desiccator except when being observed. A Siemens Elimskop 1a was used for all electron microscopy. A long focal-length double-tilt specimen cartridge kept the ferromagnetic specimens out of the field of the objective lens and thus minimized spherical aberration. The microscope was equiped with a liquid-nitrogen cold trap, which helped avoid contamination of the specimen during prolonged observation.

4.6 X-ray Diffraction

4.6.1 Theory

An oscillating-crystal technique (22,61-63) was used to determine the tetragonality of virgin and aged martensite. The technique exploits the fact that crystallographic orientation relationships exist between martensite and the parent austenite. Two sets of such relationships have been observed (64): the Kurjumov-Sachs

relationship:

$$(111)_\gamma \ || \ (110)_\alpha \qquad [1\bar{1}0]_\gamma \ || \ [1\bar{1}1]_\alpha \qquad (3)$$

and the Nishiyama relationship:

$$[111]_\gamma \ || \ [110]_\alpha \qquad [\bar{2}11]_\gamma \ || \ [1\bar{1}0]_\alpha \qquad (4)$$

The two differ by a rotation of 5° 16'. A consequence of both these relationships is that martensite may form in 24 equivalent orientations in an austenite crystal. On an austenite (001) pole figure (Fig. 6), it is found that the $(002)_\alpha$ poles are separated by 45° from the $(200)_\alpha$ and $(020)_\alpha$ poles. Specifically, $(002)_\alpha$ poles are near $(001)_\gamma$ while $(200)(020)_\alpha$ poles are near $(110)_\gamma$. Thus, in a single austenite crystal transformed to martensite, diffraction conditions will be fulfilled for the $(002)_\alpha$ planes at an angle 45° from that producing diffraction from the $(200)(020)_\alpha$ planes. This permits the recording of the diffraction of each set of planes on separate films even though the spacings of the planes are quite similar. Accordingly, the difficulty of separating the tetragonal doublet can be circumvented and the c/a ratio of martensite can be determined.

4.6.2 Specimen Preparation and Alignment

To use this "psuedo-single crystal" technique, alloys with M_s temperatures below room temperature are needed, because the parent austenite single crystal must
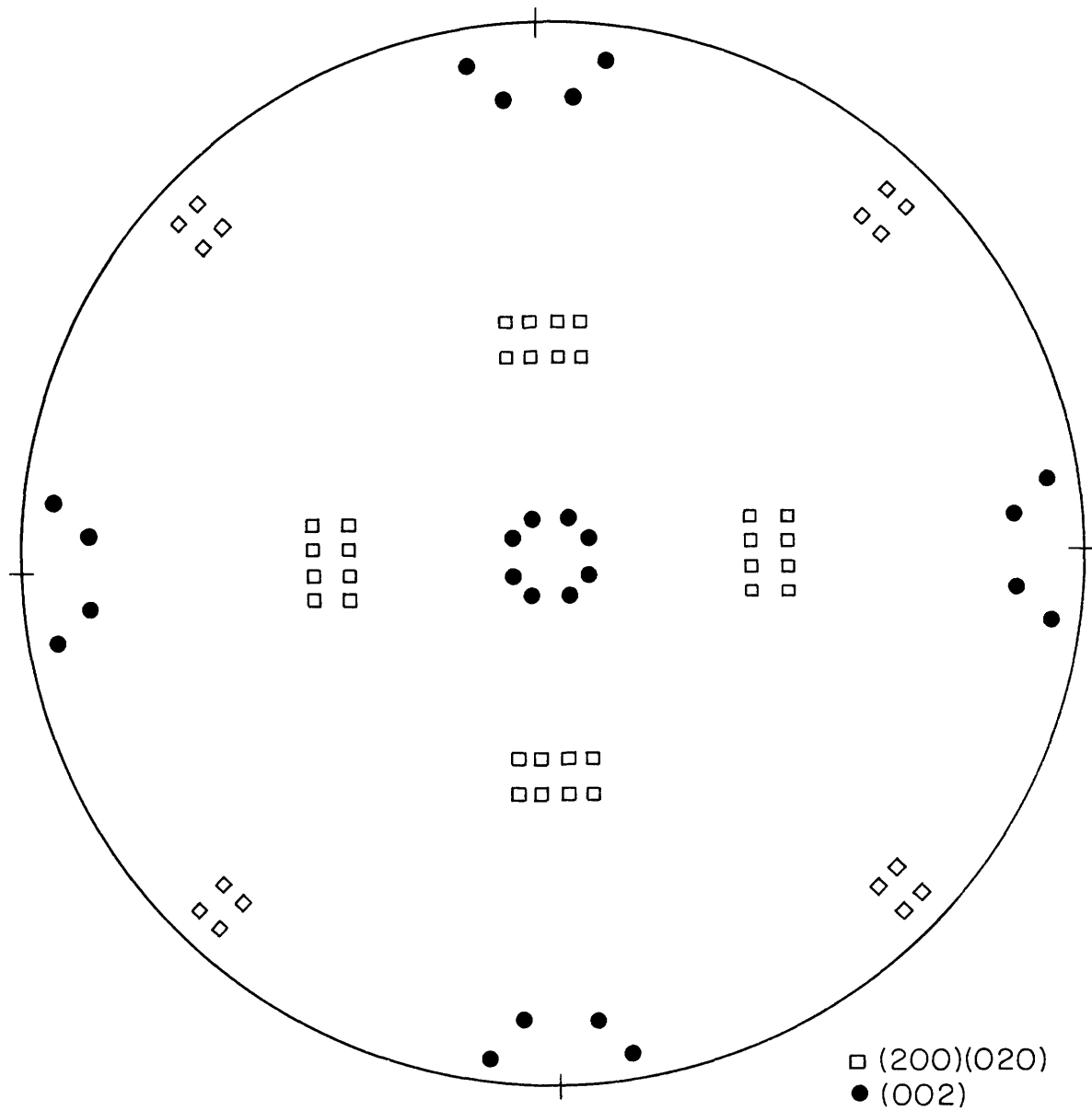
FIGURE 6. AUSTENITE (OOI) POLE FIGURE SHOWING THE (2OO)
(O2O) AND (OO2) MARTENSITE POLES IN THE
KURDJUMOV-SACHS ORIENTATION RELATIONSHIP.
(AFTER WERNER (62))

be suitably oriented to produce the desired results. Hence, only some of the alloys could be used for this work.

Three-eighth inch cubes were cut from the original hot-rolled plates. The cubes were compressed to provide a small amount of plastic upset. Then the cubes were annealed at 1350°C for 24 hours in a vacuum better than 1×10^{-5} torr and furnace colled. This treatment was usually sufficient to yield some austenite grains about 3/16 inches in diameter. Occasionally it was necessary to repeat the strain-annealing process and to use up to 3-day annealing treatments in order to obtain large grains. The size of the grains was checked by etching the cubes with Marble's reagent.

The cubes were cut in half and the largest grain from one of the cut faces was selected. This grain was removed with a combination of cutting and lapping. All cutting was done with a string saw using a wire less than 0.010-inch in diameter coated with a slurry of carborundum in oil. The lapping was done with a slurry of 1000 mesh carborundum and water. After removal, the grain was cut into individual crystals about 1 millimeter square. Each crystal was etched and optically inspected to insure that it was indeed an untwinned single crystal. Where doubt existed, a wide-spot Laue exposure was made. Any imperfect crystals were discarded.

Each crystal was dissolved in warm aqua regia until it was about 1/2 millimeter in diameter. The crystal was

then glued with Duco cement to a 0.3 millimeter diameter glass capillary. The crystal was oriented with Laue exposures, and a second capillary was glued on parallel to a $[100]_\gamma$ direction. Collodion cement (or Saueriesen in the case of specimens intended for aging treatments above $100\,°C$) was used for the second gluing operation. The first capillary was removed by dissolving the Duco cement with acetone. The oriented-crystal capillary was installed in a Supper head goniometer, which formed the specimen holder for a rotating-oscillating x-ray camera. The orientation of the crystal was checked with further Laue exposures so that the $(100)_\gamma$ pole of the austenite crystal was less than $1/2°$ from the rotation axis of the camera.

The direction of a second $\{100\}_\gamma$ pole (i.e. perpendicular to the $(100)_\gamma$ rotation axis) was determined with Laue exposures. After quenching to produce martensite, four $(002)_\alpha$ poles were approximately parallel to this $\{100\}_\gamma$ and eight $(200)(020)_\alpha$ poles $45°$ from it parallel to the $\{110\}_\gamma$ poles.

4.6.3 X-ray Exposures

The goniometer-capillary-crystal unit was mounted in a rotating camera 5.7 centimeters in diameter. The crystal could be cooled to $-100\,°C$ to transform it to martensite by a jet of cold helium gas obtained by passing the helium through a copper coil immersed in liquid nitrogen. Exposures were made with Fe K_α radiation. The expected angles of the

$(002)_\alpha$ and $(200)(020)_\alpha$ diffraction spots were calculated, and the goniometer was adjusted to oscillate about one of these angles to record one or the other set of spots. Oscillation ranges of 25 and 15° were used to record the $(002)_\alpha$ and $(200)(020)_\alpha$ spots, respectively. Exposure times were 3 hours for oscillation patterns and 15 hours for complete rotation patterns. The initial exposures were made with the specimen cold except for the time required to change films and reorient the crystal for the other set of spots. Thus, virgin martensite was observed with x-ray diffraction.

After the initial exposures the crystal was aged at temperatures ranging from room temperature up to 350°C. Heating was done with air furnaces with a temperature control of ±5°C. The specimen remained in place on the goniometer during the aging treatments. At intervals the specimen was cooled to room temperature and exposures were made to follow the course of changes due to aging.

Films produced by this method were measured with a standard Debye film measuring device, and the c and a parameters of the martensite were calculated with an accuracy of ±0.01Å. This uncertainty is due to the fact that the spots were rather broad because of the strained condition of the martensite lattice. The c/a ratio of the martensite was calculated with an accuracy of ±0.003.

Chapter V

RESULTS AND DISCUSSION

5.1 Microscopy

5.1.1 Optical Microscopy

Figures 7 and 8 follow the changes in microstructure
of lath and twinned martensites as a result of one-hour
aging treatments at temperatures up to 350°C.

The as-quenched structure of lath martensite
(Fig. 7a) consists of packets of plates, which appear to
intersect one another at about 60° angles, in accordance
with the reported (111) habit plane. (10,13,36) The sample
tempered at 100°C (Fig. 7b) etched more darkly compared
to the as-quenched specimen, indicating that some aging
reaction had taken place. When tempered at 200°C the
martensite becomes still darker etching, and some very
fine precipitates may be seen (Fig. 7c). Specimens
tempered at 300°C and 350°C (Fig. 7d and 7e) exhibit fine
carbide-particle dispersions.

The structure of the twinned martensite consists
of acicular plates ranging in size from several hundred
microns down to about 10 microns. Some of the plates have
well defined midribs. Between the plates are small regions
of retained austenite, amounting to about 10 volume percent.
This is in contrast to the lath martensite which has little
if any retained austenite. The as-quenched and 100°C
temper samples appear very much alike (Fig. 8a and 8b).

(a) Unaged, 1000X

(b) Tempered at 100°C, 1000X

Figure 7: Optical micrographs of 18Ni-0.11C Lath Martensite
aged for one hour at indicated temperatures.
1% Nital etch.

(c) Tempered at 200°C, 1000X

(d) Tempered at 300°C, 1000X

Figure 7 (continued)

(e) Tempered at 350°C, 1000X

Figure 7 (continued)

(a) Unaged, 1000X

(b) Tempered at 100°C, 1000X

Figure 8: Optical micrographs of 18Ni-0.4C Twinned Martensite
aged for one hour at indicated temperatures.
1% Nital etch.

(c) Tempered at 200°C, 1000X

(d) Tempered at 300°C, 1000X

Figure 8 (continued)

(e) Tempered at 350°C, 1000X

Figure 8 (continued)

Both have some darker etching regions. It must be remembered that the as-quenched condition in the case of both optical and electron microscopy refers to samples aged at room temperature for some days as a consequence of the techniques involved. Thus, the twinned martensite might be expected to show some evidence of tempering, i.e. dark etching, when observed as-quenched, while such effects would be less apparent in lath martensite due to the lower carbon content. The results of aging the twinned martensite at higher temperatures follow the same course as that of lath martensite. After a 200°C temper (Fig. 8c), the alloy becomes darker etching, with some slight evidence of precipitation. After tempering at 300 or 350°C (Fig. 8d and 8e), the martensite is light etching and contains dispersions of carbide particles, in greater quantity than in the lath martensite due to the higher carbon content.

5.1.2 Electron Microscopy

The structure of lath martensite after various aging treatments is shown in Fig. 9. The unaged structure is made up of laths ranging in width from 500 to 5000Å, having an internal substructure of extremely dense tangles of dislocations. After aging for one hour at 100°C the structure remained unchanged (Fig. 9b); no evidence of carbide precipitation could be seen.

Two types of carbide particles precipitated on

(a) Unaged, 44000X

(b) Tempered at 100°C, 44000X

Figure 9: Transmission electron micrographs of 18Ni-0.11C
Lath Martensite aged for one hour at indicated
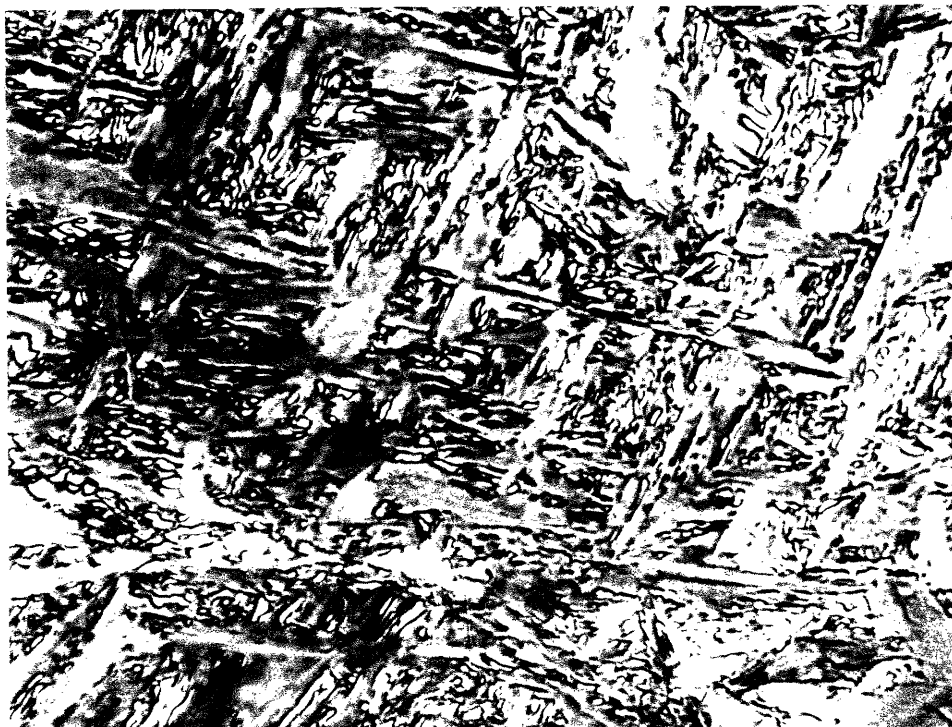temperatures.
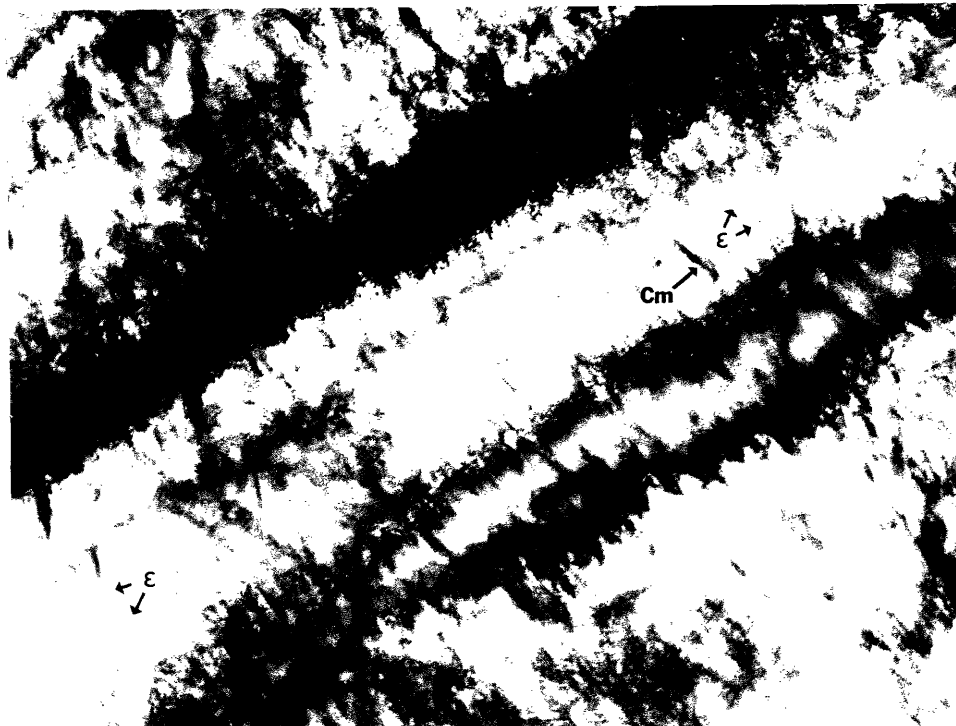
(c) Tempered at 200°C, note ε-carbide and
    cementite particles, 32000X.
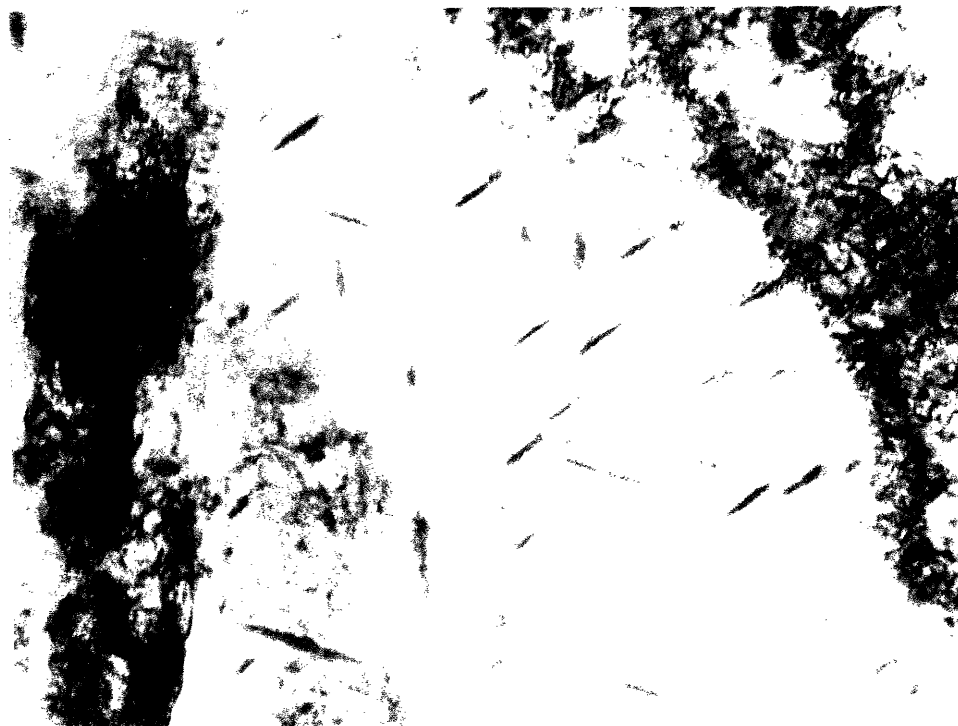
(d) Tempered at 300°C, note larger cementite
    particles, 44000X.

Figure 9 (continued)

tempering for one hour at 200 °C (Fig. 9c). One type of
carbide was present as fine needle-like precipitates a
few hundred angstroms in length separated by distances of
about 1000Å. The other carbide particles were much
larger, roughly 2000Å long, and spaced about 5000Å apart.
The finer particles conform to other observations of
ϵ-carbide (42,48), while the larger carbides resemble
cementite. (42) Because of the complexity of the structure
it was not possible to obtain enough electron-diffraction
information to positively confirm these indentifications;
however, the orientations of the particles are consistent
with the conclusion that the smaller particles are ϵ-
carbide and the larger ones cementite.

After tempering at 300°C for one hour (Fig. 9d),
there are many more cementite particles, which are now up
to 5000Å long. The dislocation density also seems to be
somewhat reduced from that of the specimens tempered at
lower temperatures. This suggests that some recovery
occurs in the lath martensite tempered at or above 300°C.

Figure 10 shows the structure of twinned
martensite after one hour at various temperatures. The
morphology of the unaged alloy consists of acicular
platelets ranging in length from less than 1 micron up to
hundreds of microns (Fig. 10a). With suitable adjustment
of the specimen tilt in the electron microscope, it was
possible to see that each platelet is internally

twinned. Diffraction results indicate that the twins
are of the {112} type, in agreement with previous results.
(10,42) The twin spacing of 60 to 100Å can be seen in
Fig. 10b. The dislocation density of the twinned martensite
must be substantially lower than that of lath martensite,
because no extensive tangles of dislocations can be seen
anywhere in the structure. Aging at 100 °C produces no
noticeable change in the structure (Fig. 10c). Occasional
small ares of retained austenite can be noted in Fig. 10c.
This is in contrast to the electron micrographs of
lath martensite, where no such regions are observed. The
sample aged at 200°C had an extensive distribution of
precipitates similar to the ε-carbide particles observed
by others. (42,48) (Fig. 10d) The carbide particles are
very thin and several hundred angstroms long. As in the
case of lath martensite electron diffraction data was
insufficient to determine unambiguously the orientation
of the ε-carbide particles. However, the results are
consistent with other observations (42,48) that ε
precipitates on {100} martensite planes. There seems to
be no cementite present after the 200°C aging as there was
in the case of lath martensite. Tempering for one hour at
300 °C produces a structure containing both ε-carbide and
cementite (Fig. 10e). At this stage the ε particles are
still in the form of thin needles up to about 2000Å long,
but are not present in nearly the same profusion as after

(a) Unaged, note mottled areas (m), 14000X

Figure 10: Transmission electron micrographs of 18Ni-0.4C
Twinned Martensite aged for one hour at indicated
temperatures.

(b) Tempered at 100°C, note fine twins (t) and mottling (m), 42000X.

(c) Tempered at 100°C, retained austenite (ra), 15000X.

Figure 10 (continued)
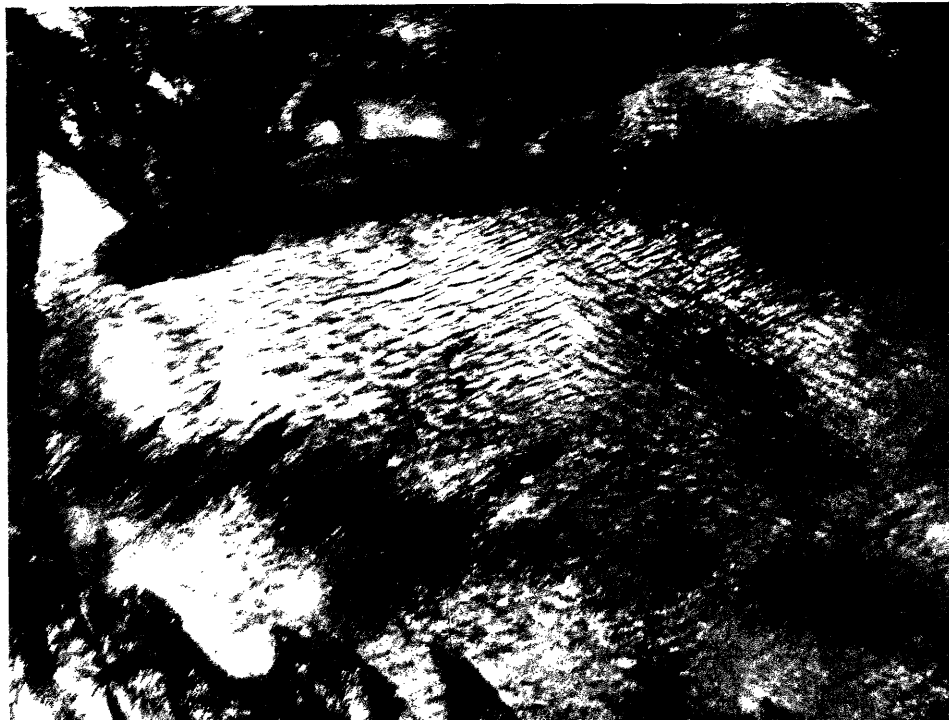
(d) Tempered at 200°C, note dispersion of
    ε-carbide particles, 14000X.
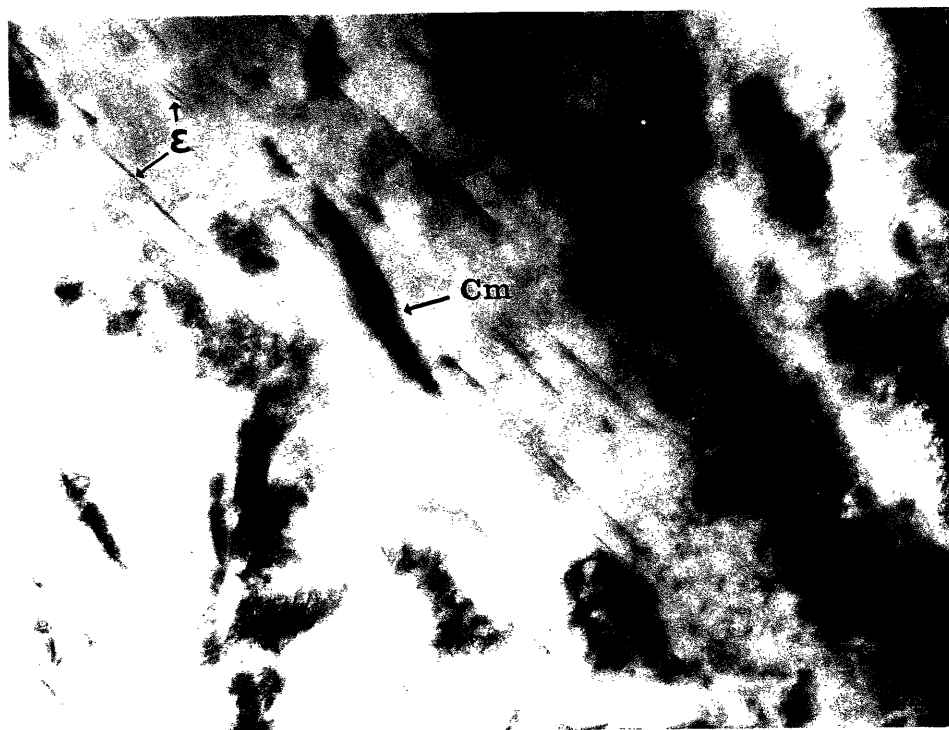
(e) Tempered at 300°C, ε-carbide and cementite
    particles indicated, 48400X.

Figure 10 (continued)

200 °C aging. The cementite particles range in size up to 5000Å long and 500 to 1000Å wide.

A subtle feature in some of the electron micrographs of martensite is the mottled appearance in various areas of the structure. While the effect is observed in both types of martensite, it is much more evident in the twinned martensite. Possibly the dislocation substructure of the lath martensite obscures the mottling. The mottling is most prevelent in the unaged and 100°C samples, in which it can be observed throughout the twinned martensite when the diffraction conditions are suitably adjusted by tilting the specimen. In specimens tempered at 200°C and higher, mottling may be seen in some areas, but not as extensively as in the samples aged at lower temperatures. Mottled structures have been noted previously in similar alloys. Eldis (44) attributed the effect to contrast from dislocations, while others (65-66) have suggested that it is due to carbon clustering or an early precipitation step before individual carbides are resolved.

The mottling in iron-nickel-carbon martensites bears a strong resemblance to the strain-contrast effect which has been called tweed, observed by Tanner et al. (67-70) in several alloy systems during the very early stages of precipitation or ordering. The observation of the tweed structure is accompanied by an asymmetric

broadening of electron diffraction spots. It is thought
that the tweed phenomenon occurs because clusters of solute
atoms develop prior to the actual emergence of precipitate
particles. The clusters are coherent with the matrix and
the coherency strains give rise to the diffraction effects
observed. When the clusters grow large enough to become
precipitate particles the tweed structure gradually
disappears. Substructures and diffraction effects similar
to tweed are found in some systems undergoing spinodal
decomposition. (71)

In order to determine whether a phenomenon
similar to tweed, involving the clustering of carbon atoms,
is at play during the aging of martensite, a specimen
tempered for one hour at 150 °C is of special interest
(Fig. 11). The structure has regions with coarser
mottling than seen in other specimens and areas with
ε-carbide particles. Those areas with more clearly
resolvable carbide particles are distinctly freer of
mottling than the surrounding areas. Moreover, the
texture of the mottling seems to lie parallel to the
orientation of the carbide particles. The texture of the
mottling in the unaged and 100°C aged specimens is also
frequently observed to be consistent with a parallelism
to $\{100\}_{\alpha'}$ planes which ε-carbide is known to form on.
The spots of the coresponding electron diffraction pattern
are asymmetrically distorted (Fig. 11b and 11c). Thus,
the similarities to tweed are striking. However, these

(a)

(b)

(c)
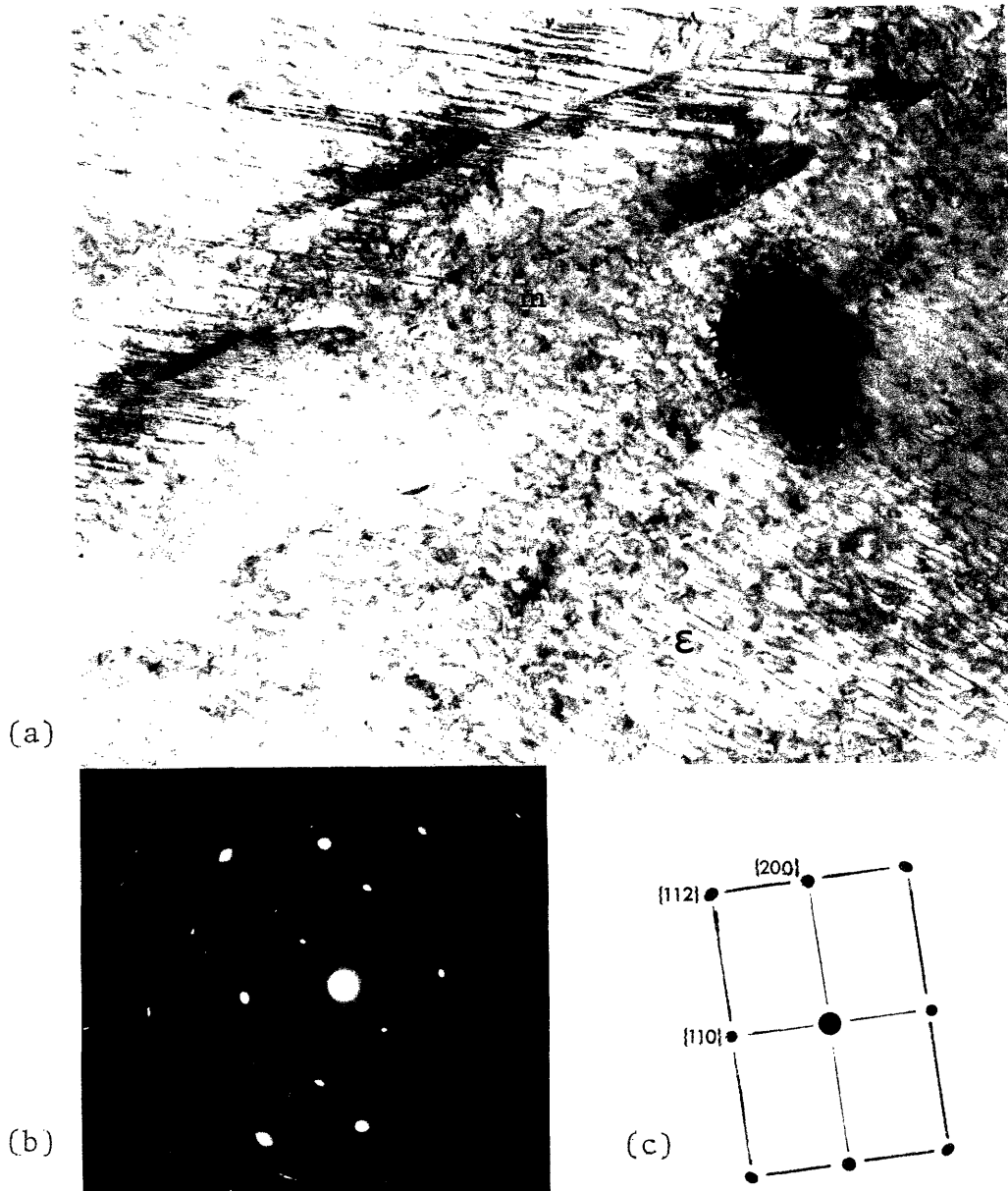
Figure 11: 18Ni-0.4 Twinned Martensite tempered at 150°C for one hour. a) transmission electron micrograph, ε-carbide particles and coarse mottling (m) indicated. 38000X. b) associated (110) electron diffraction pattern suitably oriented. c) solution of diffraction pattern, note asymmetrically distorted spots.

observations alone are not sufficient to allow an unambiguous conclusion that the mottling is due to carbon clustering prior to carbide precipitation; nevertheless, they do offer some evidence that this is the case.

5.2 X-ray Diffraction Results

Exposures made on unaged martensite quenched and held at about -100°C using the "psuedo-single crystal" technique showed that the structure of virgin martensite is body-centered tetragonal. The c/a ratios obtained were combined with those obtained by Winchell (22) using the same x-ray technique. Winchell's results include many lower-carbon alloys thus extending the range of data. The c/a ratio varied linearly with carbon content (Fig. 12). A least squares fit of the data points produced the equation:

$$(c/a)_{\alpha'} = 1.005 + 0.057(w/o \text{ C}) \tag{5}$$

The slope of this equation is somewhat higher than the slope of 0.045 previously reported for Fe-C alloys. This may be due to nickel affecting the way in which carbons expand the lattice, or it may be due to some systematic error introduced by the x-ray technique.

The a and c lattice parameters obtained from the present results also varied linearly with carbon:

$$(c)_{\alpha'} = 2.867 + 0.122(w/o \text{ C}) \tag{6}$$

$$(a)_{\alpha'} = 2.821 - 0.010(w/o \text{ C}) \tag{7}$$

63
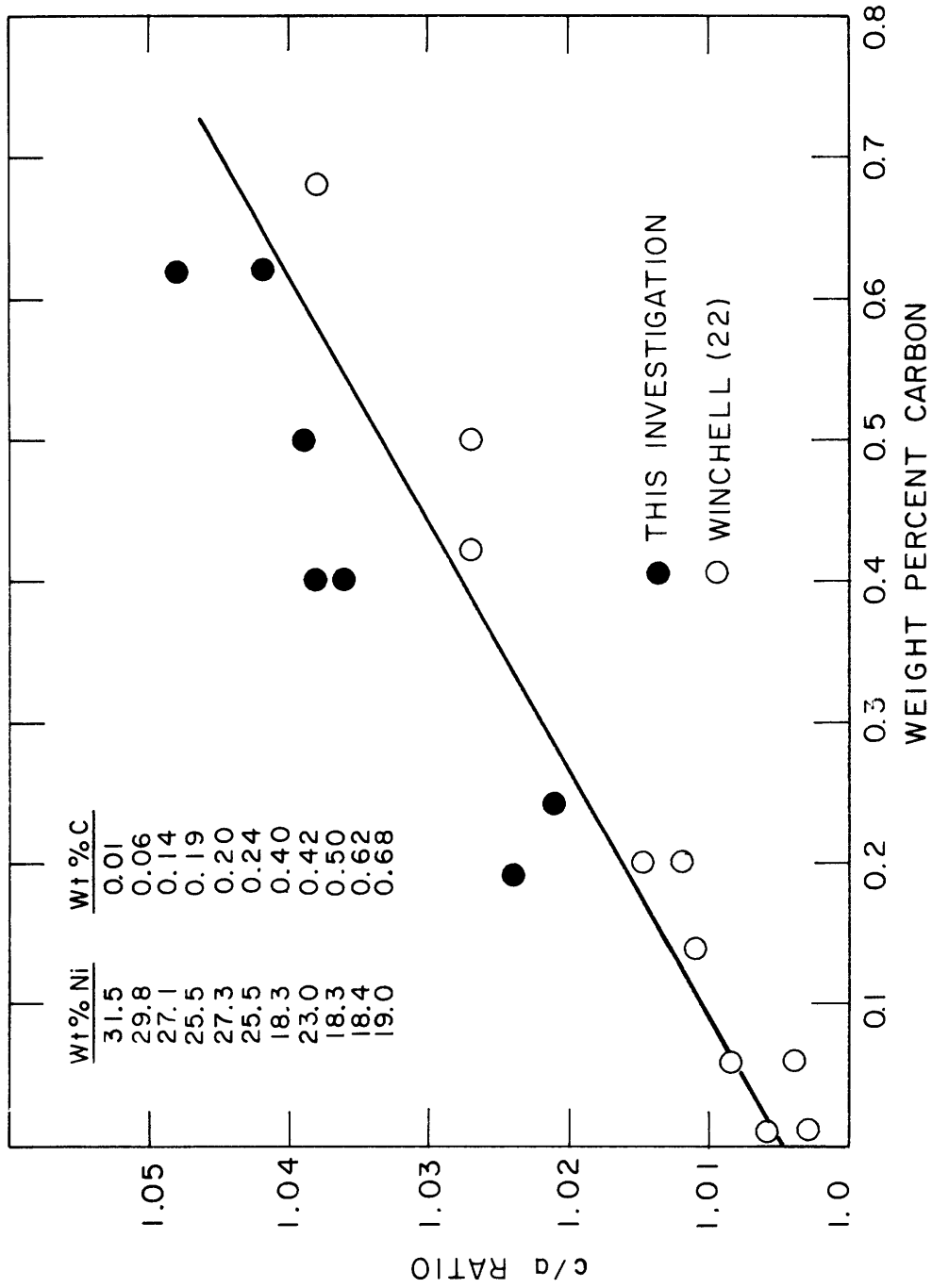
FIGURE 12 c/a RATIO OF VIRGIN MARTENSITE AS DETERMINED FROM
AUSTENITE SINGLE CRYSTALS TRANSFORMED AND X-RAYED
AT ABOUT -100°C

These results are in good agreement with previous measurements of martensite lattice parameters, except for the zero carbon intercept of the a parameter, which is somewhat lower than reported elsewhere. (63) This is probably due to the inherent errors of the technique, but may be a manifestation of the reported decrease (72) in lattice-parameters of Fe-Ni alloys in this range of nickel contents (18 to 24w/o).

Because the crystals must be austenitic at room temperature to allow the necessary alignments prior to quenching, only alloys with subambient M_s temperatures could be used for these x-ray measurements. Unfortunately, no alloys could be found with lath martensite having subambient M_s temperatures. Consequently, the lattice-parameter data are based on twinned martensites.

After aging at temperatures ranging from room temperature to 100 °C, a new set of (002) spots appears coresponding to a smaller c parameter than that of virgin martensite (α'). The intensity of the new set of spots increases with aging time, while the $(002)_{\alpha'}$ spots' intensity decreases and finally disappears. The complete disappearance of the $(002)_{\alpha'}$ spots takes up to 40 days of room temperature aging, but less than 15 minutes at 100 °C. The new (002) spots are noticeably broader than the $(002)_{\alpha'}$ spots. The (200)(020) martensite spots broaden in the direction of a larger a-parameter during aging, suggesting that it also splits into two separate spots. The emergence

of the smaller c-parameter and the shifting of the (200)(020)
position show that a low- or nil-carbon martensite forms
with a c/a ratio of 1.004±0.001 independent of the alloy
content. We will call this martensite α_t, for transition,
since it forms as an intermediate step in the overall
decomposition:

$$\alpha' \rightarrow \alpha_{bcc} + Cm \qquad\qquad (8)$$

The activation energy for the formation of α_t was
estimated in the following way: By visual inspection of the
x-ray films, it was possible to determine the aging times
necessary to achieve equal intensities of the $(002)_{\alpha'}$ and
the $(002)_{\alpha_t}$ spots as well as the times for the complete
disappearance of the $(002)_{\alpha'}$ spots. These conditions
corespond to the half-way point and the completion of the
formation of α_t respectively. A plot of natural log time
vs. reciprocal aging temperature was constructed, and the
slope of the plot times R, the gas constant, was taken to
be Q, the activation energy, for the process. The
activation energies thus obtained were 21 kcal per mole
for both stages of the $\alpha' \rightarrow \alpha_t$ transformation.

The formation of α_t entails the redistribution
of carbon atoms from the single set of octahedral sites
they occupy in the virgin martensite to other positions where
they do not expand the lattice in the original way. Previous
observations of the formation of low-tetragonality
martensite during tempering have led to the conclusion that
ε-carbide forms simultaneously and that α_t is in metastable

equilibrium with the carbide. (29,38-40) This conclusion is not supported by the present data because the electron microscopy results show that ε-carbide does not precipitate on aging for one hour at 100°C. Since the formation of α_t is complete within 15 minutes at 100°C, the carbon atoms cannot be going into the formation of carbides when α_t forms. Furthermore, the activation energy for the precipitation of carbides during tempering is reported to be about 33 kcal per mole, which is much higher than that observed in the present case for the formation of α_t.

Several other ideas about the formation of α_t involve carbon atoms moving to various types of sites from their initial locations in virgin martensite. These movements can be accomplished by diffusive jumps whose activation energy agrees closely with the observed 21 kcal per mole. One such mechanism is the randomization of carbon occupation among the three sets of octahedral sites, leading to a body-centered cubic structure expanded uniformly by carbon. Clearly, this is not the case because such martensite would have a c/a ratio of unity and a larger lattice parameter than the carbon-free lattice parameter of 2.866Å, neither of which is observed. Also such a process should happen continuously giving rise to a broadening of the $(002)_{\alpha'}$ spots rather than a discontinuous separation of α' and α_t spots.

Another possible mechanism for the $\alpha' \rightarrow \alpha_t$ transition is the segregation of carbons to dislocations

or other preferred sites. The driving force for this reaction would be a reduction in the free energy due to the lattice strains caused by carbon atoms in octahedral sites. Estimates of the capacity of dislocations for such carbon absorption have shown that about 0.20 weight percent carbon can be accomodated by the dislocation densities of 10^{12} cm^2/cm^3 thought to be present in martensite. (46) A model proposed by Lement and Cohen (59) could account for the discontinuous appearance of α_t by postulating a low-carbon region surrounding dislocations which grows as aging continues. The c/a ratio of 1.004 would be caused by tetragonal distortions of a small carbon concentration remaining in the matrix.

Another mechanism for the formation of α_t is clustering of carbon atoms. This possibility will be more fully discussed in the following sections; for the moment it will suffice to describe how α_t can develop as a result of clustering. The formation of clusters would remove carbons from the usual octahedral sites. This might occur by the same depleted-zone process as in dislocation segregation, thus giving the discontinuous appearance of α_t spots. The 1.004 c/a ratio would be due to residual carbons in matrix lattice sites or to some sort of general expansion caused by the small coherent clusters themselves. Actually, both clustering and dislocation segregation could be operative simultaneously,

but as carbon content increases clustering should
predominate due to the saturation of all available
dislocation sites early in the transformation.

5.3 <u>Resistivity</u> <u>Changes</u> <u>During</u> <u>Aging</u>

Complete sets of resistivity vs. time curves for
the five alloys of the iron-18 nickel series of alloys
are presented in Fig. 13. The results obtained from the
other alloys were entirely consistent with those presented
here. Because of the long times required for generating
the data, the curves, in most cases, were obtained in a
single run. However, where duplicate runs were made, there
was close agreement.

The data contained in the resistivity vs. time
plots have been normalized to correct for scatter of up
to ±4 percent in the initial resistivities of the
specimens. The sources of such scatter were:

1. Errors of up to 2 percent in the
measurements of the dimensions of
the specimens.

2. The 5 to 15 percent retained austenite
in the higher-carbon alloys having
twinned martensite.

3. Inadvertant straining of the specimens
due to deformation during quenching.

A least-squares plot of initial resistivity vs. carbon
content (at 18 weight percent nickel) was constructed
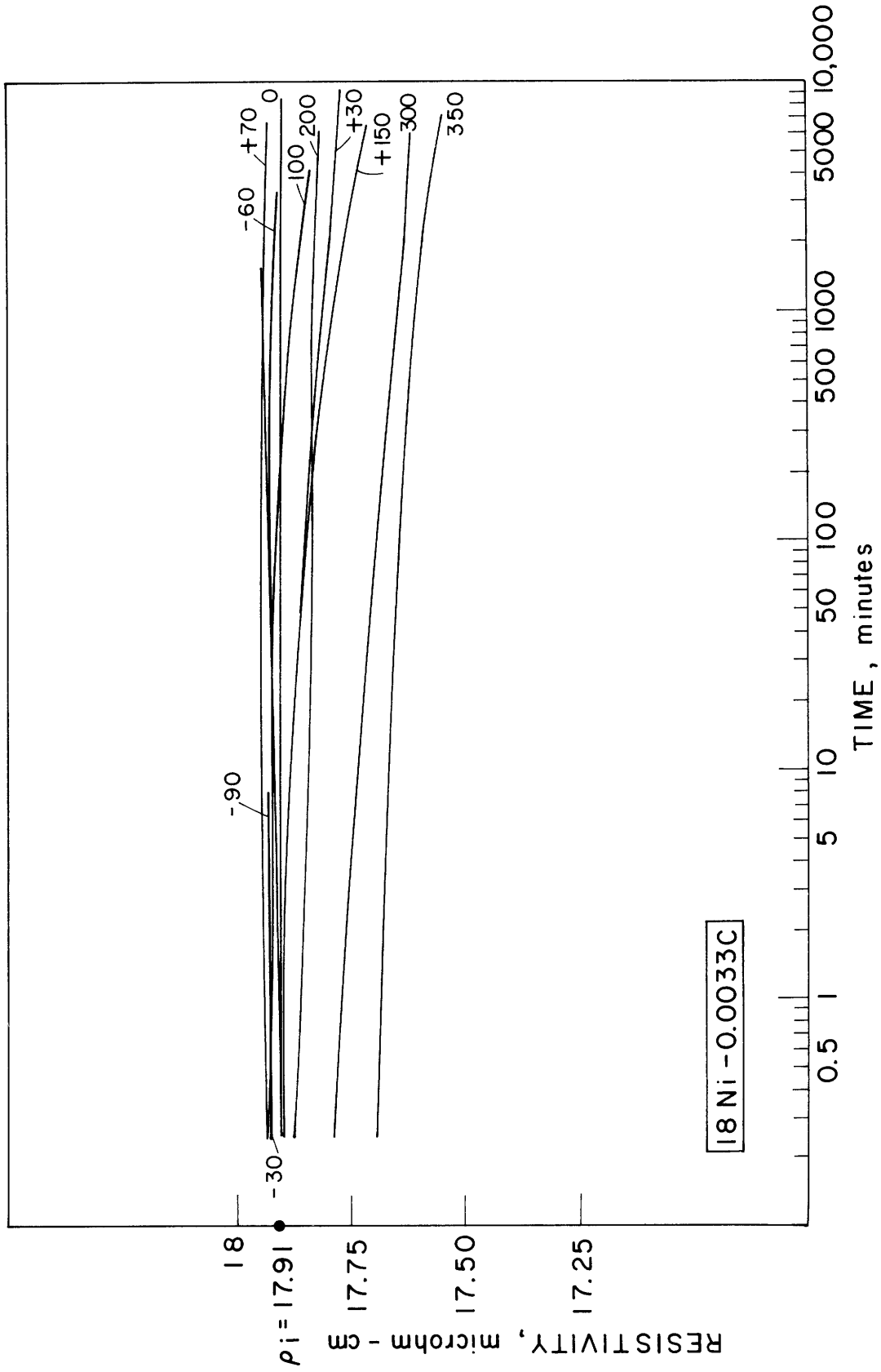
FIGURE 13a RESISTIVITY VS. TIME CURVES FOR AN 18Ni-0.0033C ALLOY AGED
AT INDICATED TEMPERATURES
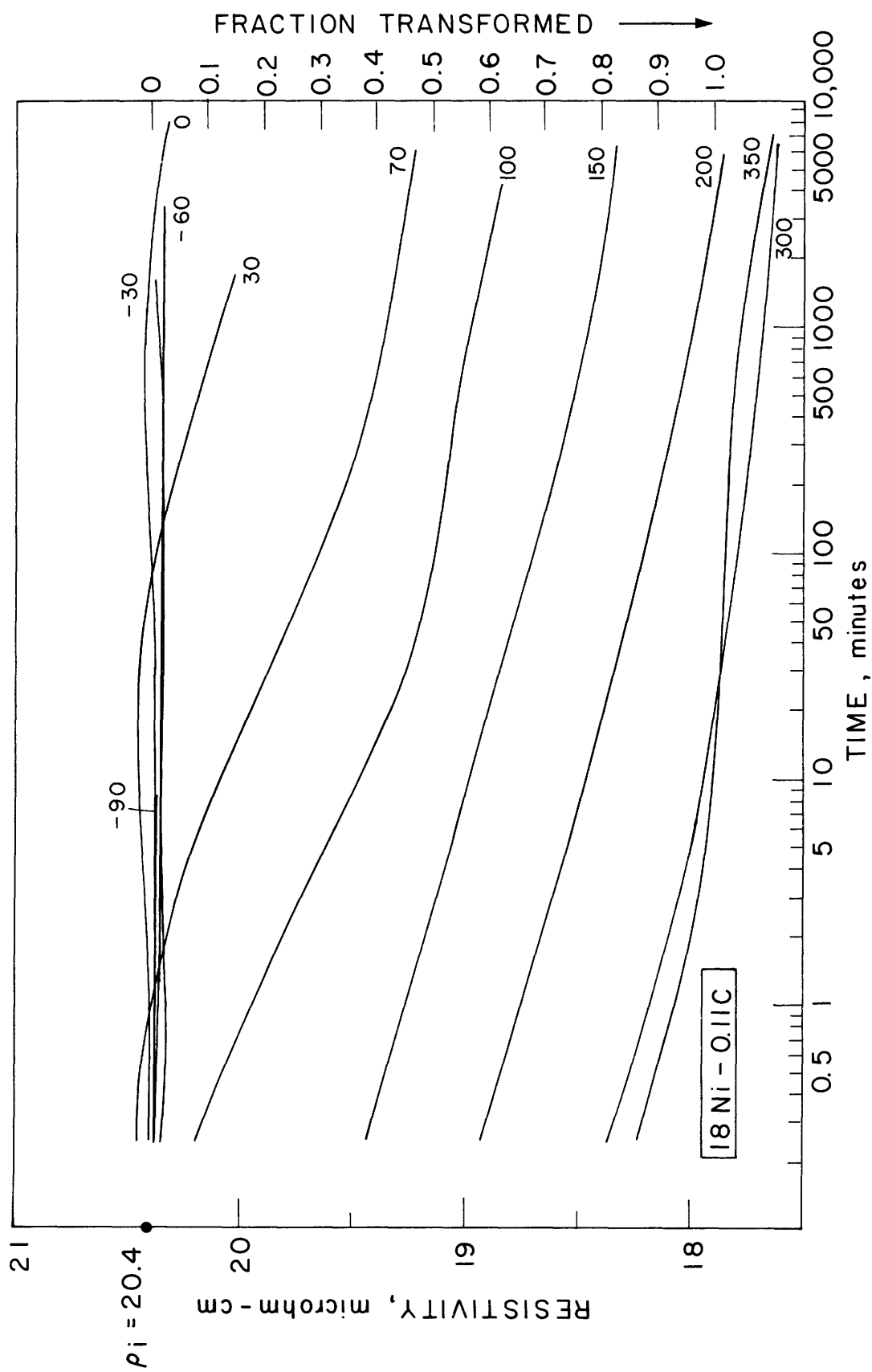
FIGURE 13b RESISTIVITY VS. TIME CURVES FOR AN 18Ni-0.11C ALLOY AGED
AT INDICATED TEMPERATURES

71
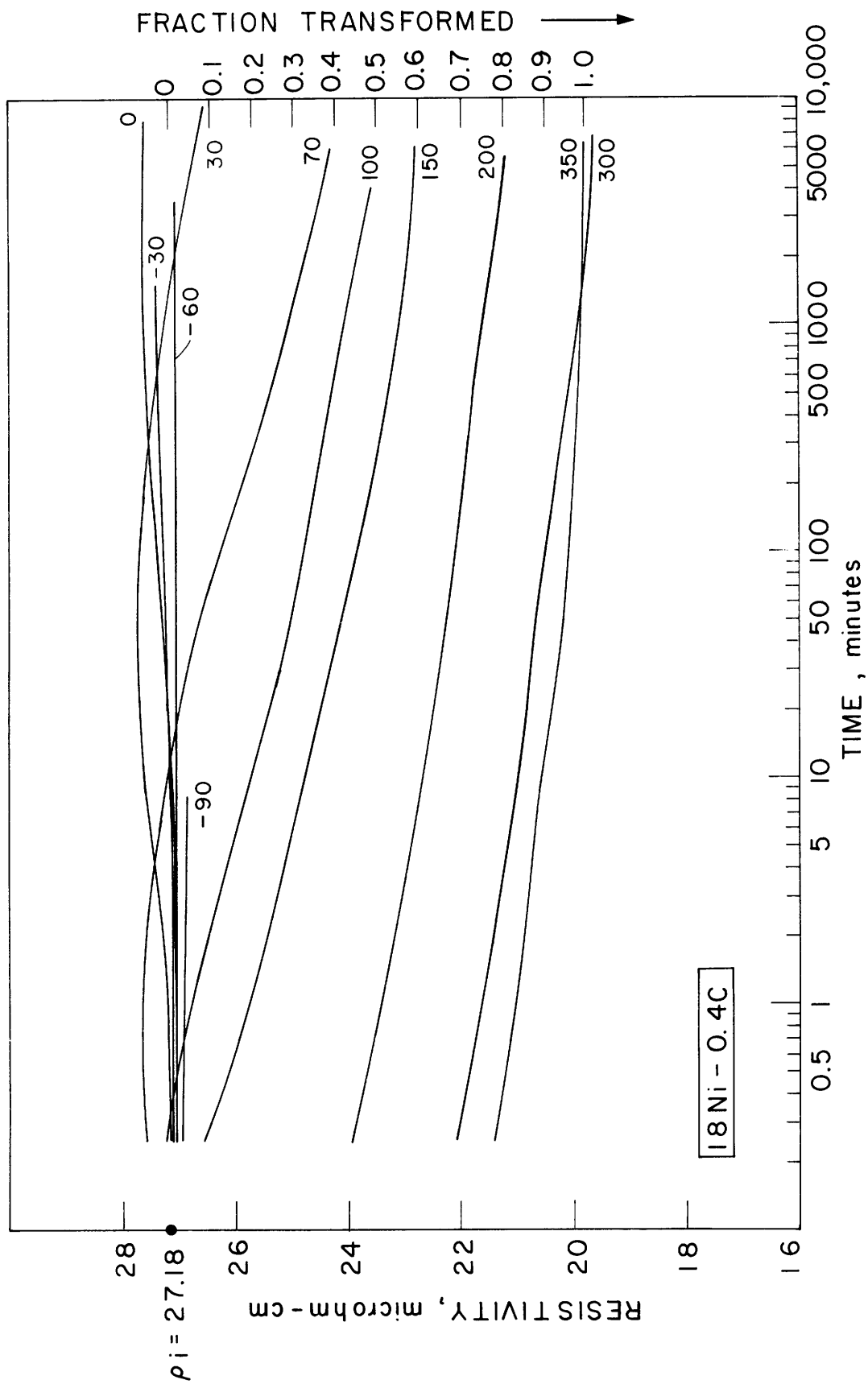
FIGURE 13c RESISTIVITY VS. TIME CURVES FOR AN 18Ni-0.4 C ALLOY AGED
AT INDICATED TEMPERATURES
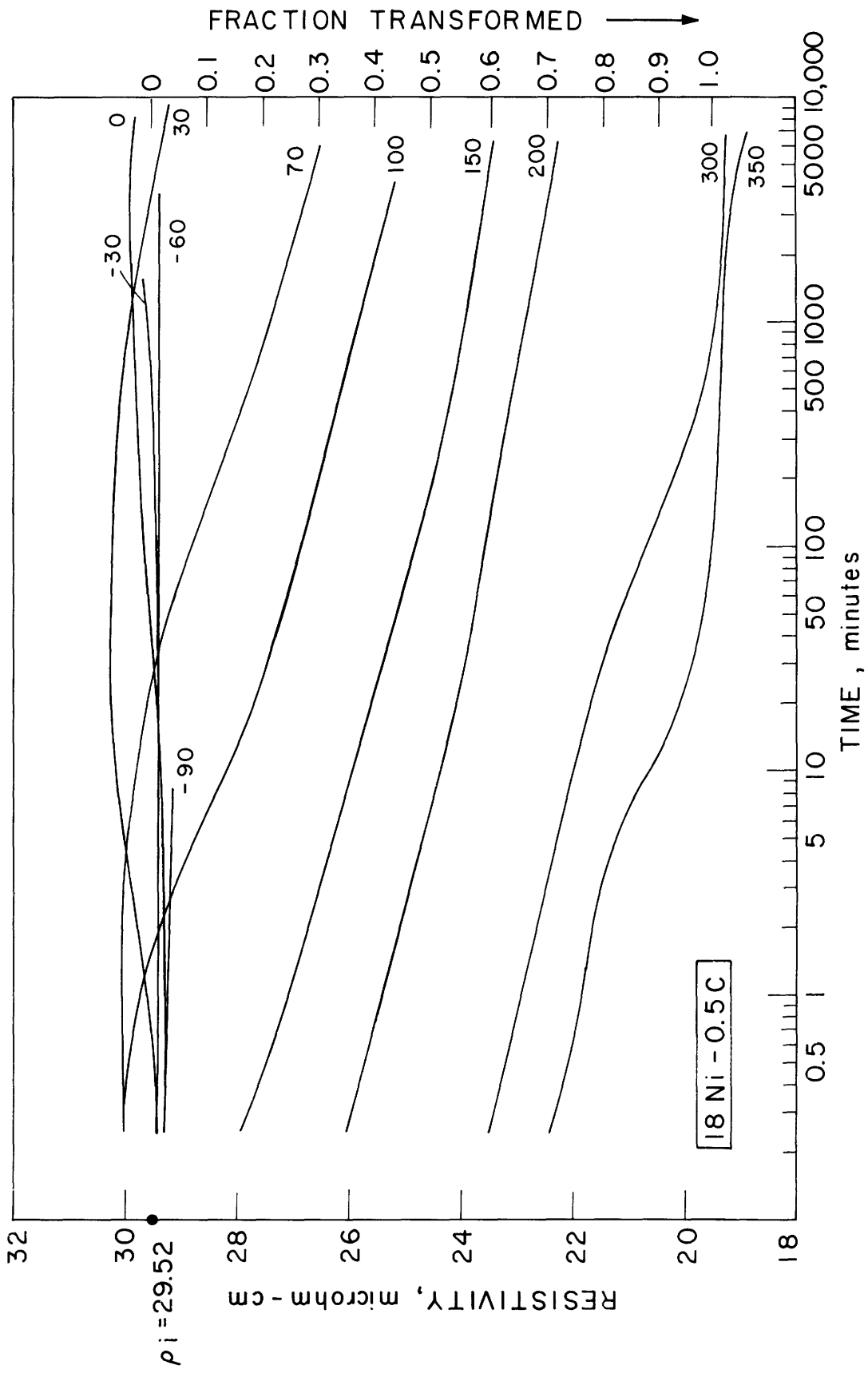
FIGURE 13d RESISTIVITY VS. TIME CURVES FOR AN 18Ni-0.5C ALLOY AGED
AT INDICATED TEMPERATURES
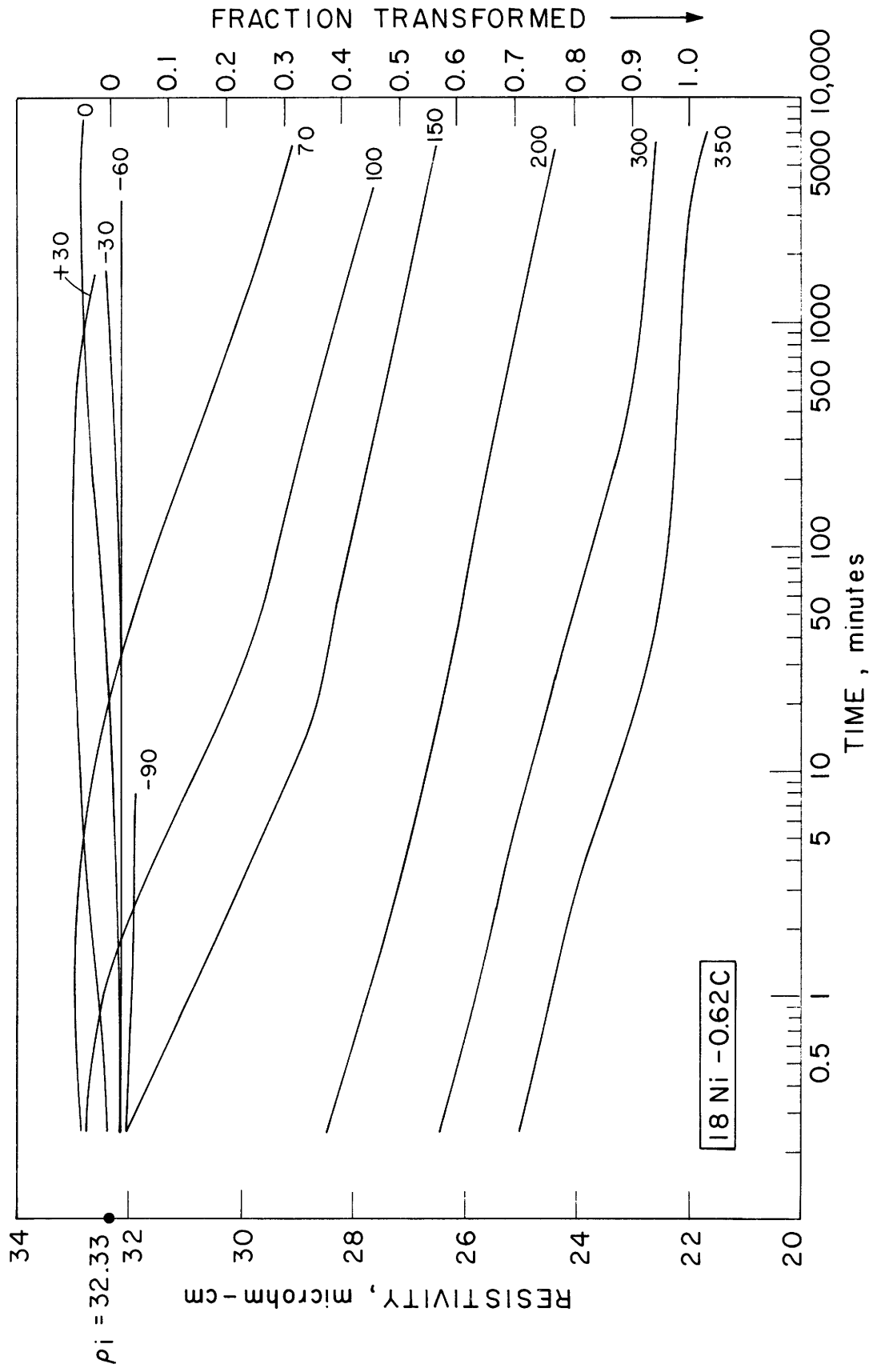
FIGURE 13e RESISTIVITY VS. TIME CURVES FOR AN 18Ni-0.62 C ALLOY AGED AT INDICATED TEMPERATURES

yielding:

$$\rho_i = 17.83 + 22.38(\text{w/o C}) \tag{9}$$

in which ρ_i = initial resistivity.

Then the resistivity values obtained during the aging of
each specimen were multiplied by the factor:

$$\rho_t = \frac{\rho_i}{\rho_o} \rho_t' \tag{10}$$

where ρ_i is obtained for each alloy from equation 9

    ρ_o = initial resistivity of a given sample

    ρ_t' = measured resistivity of sample after aging for

        time t

    ρ_t = corrected resistivity after aging for time t.

The corrected values, ρ_t, are those used in the plots
of resistivity vs. time.

Except for the 0.0033 weight percent carbon alloy,
which exhibited only slight decreases in resistivity at the
higher aging temperatures and long times, the behavior of
all the alloys was qualitatively the same. For purposes
of discussion, the curves can be divided into three regions
as shown schematically in Fig. 14. Region I is
characterized by a slight decrease in resistivity of short
duration occurring only during aging at low temperatures.
In Region II there is a resistivity peak which occurs in
alloys aged in the vicinity of room temperature. Region III
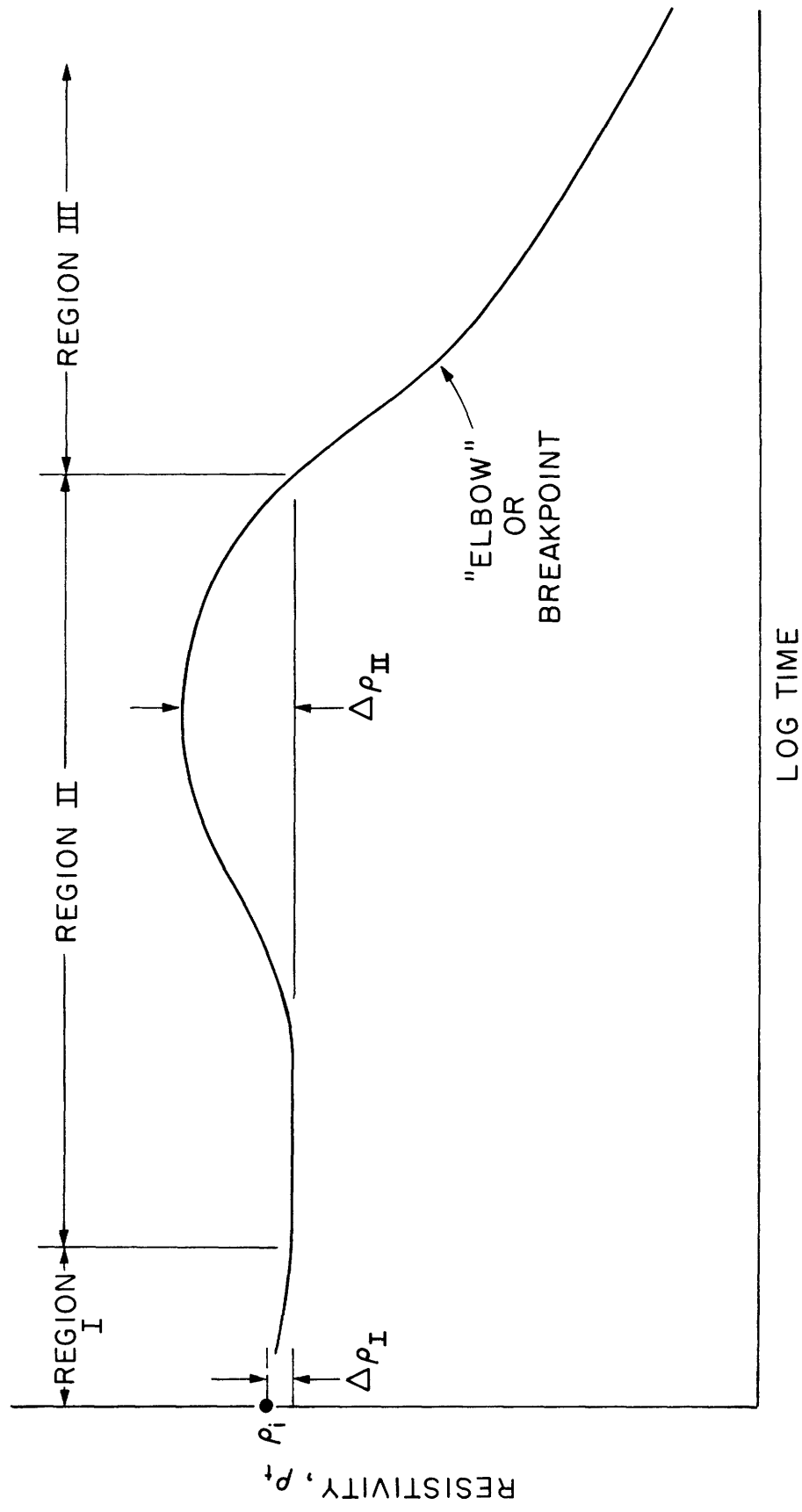
FIGURE 14 SCHEMATIC RESISTIVITY VS. LOG TIME CURVE

consists of a continuous decrease in resistivity and constitutes the only observable behavior on tempering at 100 °C and above. The next section will show that the resistivity changes are a measure of the extent of reactions taking place in the martensite as a result of aging, and that they can provide information about the activation energy and nature of the processes involved.

5.3.1 Theoretical Background

According to the quantum model for the conduction of electrons in metals, the resistivity of a perfect crystalline metal at absolute zero temperature should be zero, because the electrons travel in the perfectly periodic potential field of the lattice. (73) If the periodicity of the potential field of the lattice is disturbed, then scattering of electrons will occur giving rise to electrical resistivity. At temperatures above absolute zero, the atoms are not stationary but vibrate about their equilibrium positions, thus perturbing the lattice potential field and leading to the observed increase of resistivity with temperature of all metals. Aside from lattice vibrations, there are other factors which may cause increased resistivity due to interuptions in lattice periodicity. In a consideration of the resistivity of martensite during aging, we must take into account defects such as dislocations, interstitial and substitutional solute atoms as well as retained austenite

and precipitate phases. Each of these features, when present, leads to a disruption of the potential field of the iron lattice. Dislocations, solute atoms and coherent precipitate particles cause displacements of iron atoms from equilibrium positions. Retained austenite and precipitate particles (both coherent and incoherent), due to their different structures, have different electronic potential fields.

The contribution of defects to resistivity is independent of temperature as expressed by Matthiessen's rule:

$$\rho = \rho_t + \rho_o \qquad (11)$$

which separates the resistivity of a metal into a thermal component (ρ_t) whose origins are lattice vibrations and a defect component (ρ_o). Since all our resistance measurements were made at -196 °C, variations in resistivity must be attributed primarily to changes in ρ_o rather than in ρ_t. This means that changes in resistivity observed during aging are reflections of structural changes in the martensite.

Nordheim's rule:

$$\rho_r(x) = Ax(1-x) \qquad (12)$$

in which $\rho_r(x)$ = resistivity contribution of solute atoms of concentration x, and A is a constant, may be applied to

the dilute solution of carbon in martensite. Since x is
small the rule can be approximated as:

$$\rho_r(x) = Ax \qquad (13)$$

which means that the resistivity of virgin martensite,
with all carbons in octahedral sites, should increase
linearly with carbon content. That the initial resistivities
of the martensites formed in our alloys do increase linearly
with carbon content is an indication that we are starting
essentially from the virgin condition. Fig. 15 shows how
the initial resistivities vary with carbon content for the
three series of iron-nickel alloys. The resistivity at
zero carbon content decreases as nickel content increases,
in agreement with previous measurements at -196°C of
Fe-Ni alloys. (74)

The source of the resistivity increase due to
carbon interstitials in virgin martensite is a large
mean-square static displacement, $\bar{\mu}^2$, of the iron atom
neighbors. The larger resistivity contribution per weight
percent carbon as nickel content is increased may be
attributed to increased iron-atom displacements around
each carbon atom in the presence of nickel. The lattice
parameter of iron-nickel martensite decreases with nickel
content in the range of 18 to 25 weight percent nickel. (72)
This means a carbon atom must displace the surrounding
atoms relatively more in alloys with higher nickel. Also,
the elastic constants of iron-nickel alloys decrease as
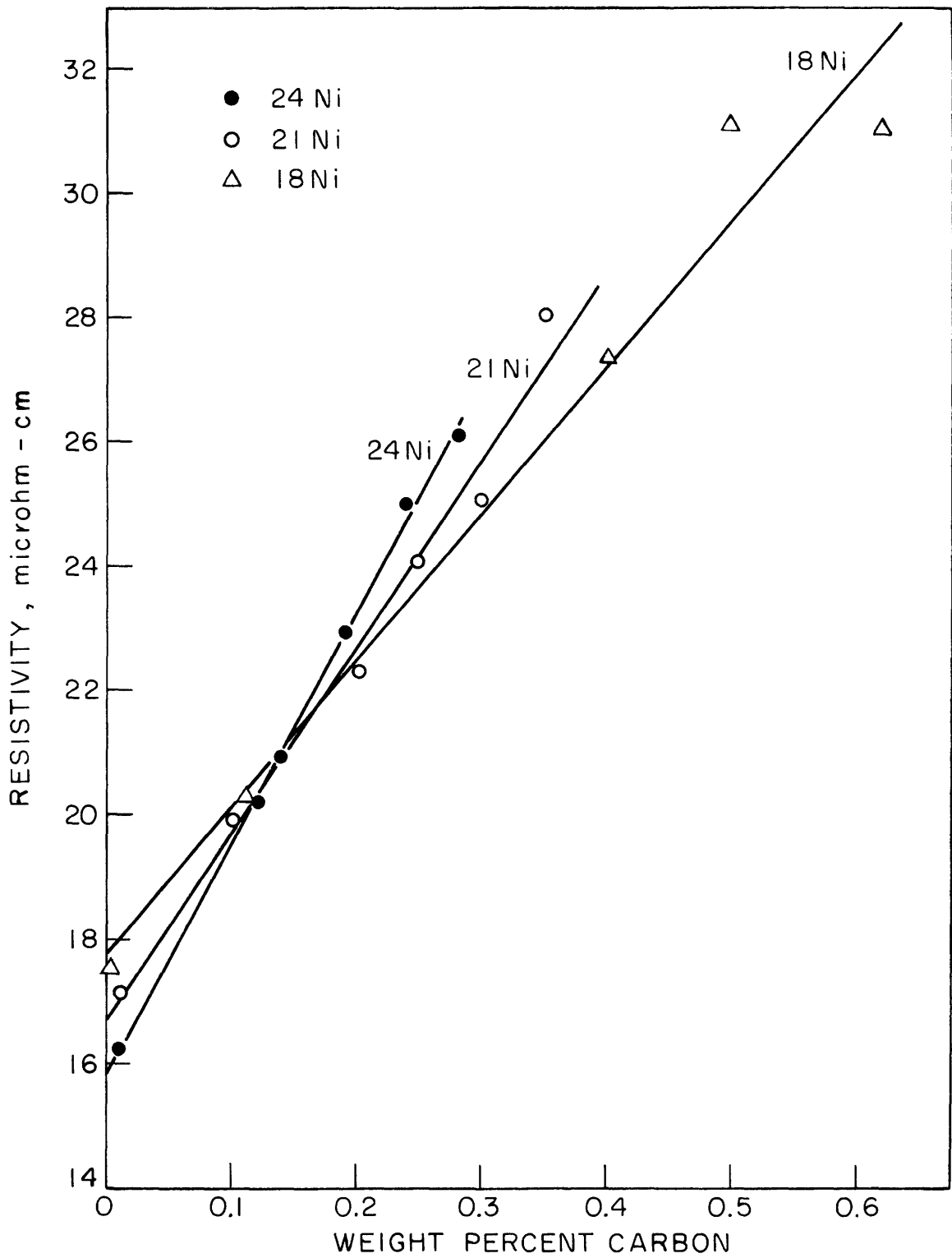
FIGURE 15. INITIAL RESISTIVITY AS A FUNCTION OF CARBON CONTENT

nickel content rises (75-76) making it easier for a carbon atom to distort the lattice.

Since the aging of martensite is largely a process of carbon-atom depletion from the iron lattice to form carbides, it is possible to follow the extent of aging by resistivity measurements. In particular, decreases in resistivity signal a reduction in iron-atom static displacements, indicating that fewer carbons remain in solution. By Nordheim's rule we may infer that such decreases are approximarely linear with respect to the amount of carbon removed from solution either to form carbides or to occupy sites such as dislocations or clusters.

5.3.2 Calculation of Activation Energies from Resistivity Data

To obtain the activation energy of a thermally activated process, one procedure is to start with a general Avrami type equation:

$$f = 1-\exp[-(kt)^n] \tag{14}$$

in which   f = fraction transformed

        t = time

        n = time exponent

  and k = $k_o\exp(-Q/RT)$ (15)

  where Q = activation energy

      R = gas constant

      T = absolute temperature

k_o = a constant

It is usually assumed that k and n are independant of f, and by taking the natural log of both sides of the equation twice:

$$\ln t = \frac{Q}{R}(1/T) + C(f) \tag{16}$$

where C is a constant for any value of f. Then the slope of a plot of ln t vs. 1/T for a given value of f gives the activation energy:

$$\frac{Q}{R} = \left(\frac{\partial \ln t}{\partial (1/T)}\right)_{f=f_1} \tag{17}$$

Values of Q thus obtained will be the same for all values of f_1 if the activation energy does not vary during the course of the transformation. If the activation energy does vary, then Q will represent an average activation energy for the process up to $f = f_1$.

Hillert (77) has pointed out that in the tempering of martensite, Q is not independant of f, since there are several overlapping steps, each possibly having a different activation energy. Consequently, he suggested that the Q value for each step can be more accurately determined by considering the transformation rate $(\partial f/\partial t)$ rather than only time to attain a given amount of transformation. In order to obtain the activation energy at $f = f_1$ Hillert considers the rate of transformation to

be a function of both f and T:

$$\frac{\partial f}{\partial t} = G(f,T) = G_0(f) \exp\left[-\frac{Q(f)}{RT}\right] \tag{18}$$

Taking the natural log of each side:

$$\ln \left.\frac{\partial f}{\partial t}\right|_{f=f_1} = \ln G_0(f_1) - \frac{Q(f_1)}{RT} \tag{19}$$

Thus, the slope of $\ln \left.\partial f/\partial t\right|_{f=f_1}$ vs. $1/T$ will give Q values

more closely reflecting the activation energy of the

process(s) going on at $f = f_1$ because

$$\frac{Q(f_1)}{R} = -\left(\frac{\partial \ln \left(\frac{\partial f}{\partial t}\right)}{\partial (1/T)}\right)_{f=f_1} \tag{20}$$

Clearly, the Hillert method is preferred when the nature

of the data allows a determination of $\left.\partial f/\partial t\right|_{f=f_1}$ at several

temperatures.

5.3.3 Region-I Initial Resistivity Drop

The initial resistivity drop ($\Delta\rho_I$) occurs only

in specimens aged at subambient temperatures, and then only

in very short times. In a given alloy $\Delta\rho_I$ decreases

linearly with increasing aging temperature (Fig. 16). The

drop does not occur in alloys with nil carbon, and increases

as carbon and nickel content are increased. These trends

may be due to autotempering since the alloys with less

carbon and nickel have higher M_s temperatures and hence may
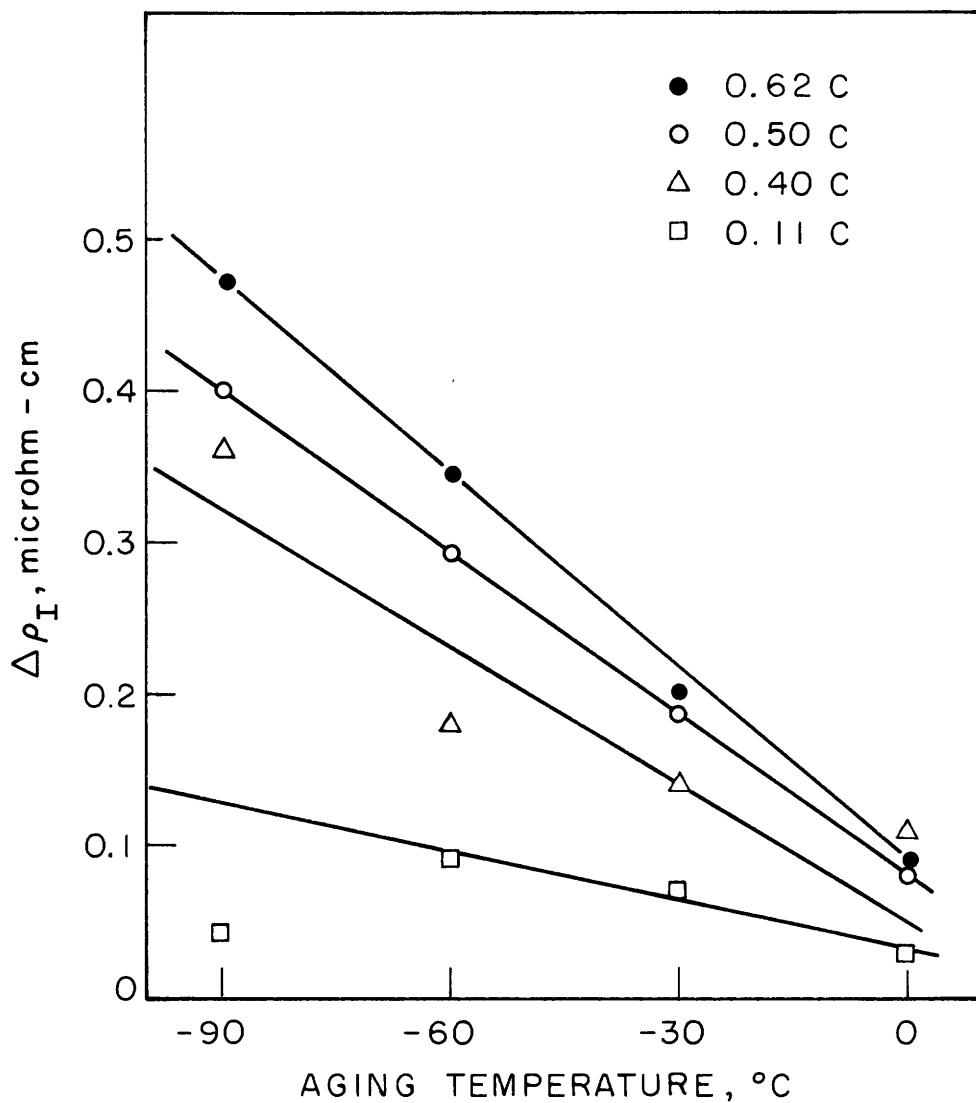
FIGURE 16. VARIATION OF INITIAL RESISTIVITY DROP
WITH AGING TEMPERATURE FOR Fe-18Ni
ALLOY OF SEVERAL CARBON CONTENTS

undergo part of the resistivity drop during the quench. This idea is supported by considering a plot of $\Delta\rho_I$ vs. carbon content for alloys with equal M_s temperatures (Fig. 17), where $\Delta\rho_I$ now becomes smaller with increasing carbon. The existence of Region I is a good indication that the martensite is in its virgin condition at the start of testing, since appreciable aging due to auto-tempering or inadvertent warming would have aged past the drop before the start of the test run.

The activation energy for the drop constituting Region I was determined by applying equation 17 to plots of log time to complete the drop or half of the drop vs. $1/T$.* A value of 3 kcal per mole was obtained, independent of alloy content. Because of the time-temperature range in which the drop occurs, only the resistivity data provides evidence of Region I, and so it is difficult to determine the cause of the drop in resistivity. Carbide precipitation or any other process involving diffusion of carbon or nickel is quite improbable because the activation energy is much too low. The possibility of retained-austenite transformation can also be discarded, because the drop occurs in lath martensite which has very little retained austenite. Furthermore, Eldis (44), who observed a similar drop, saw no change in amount of retained austenite as a result of aging in

*The data for $\Delta\rho_I$ were insufficient to apply equation 20.
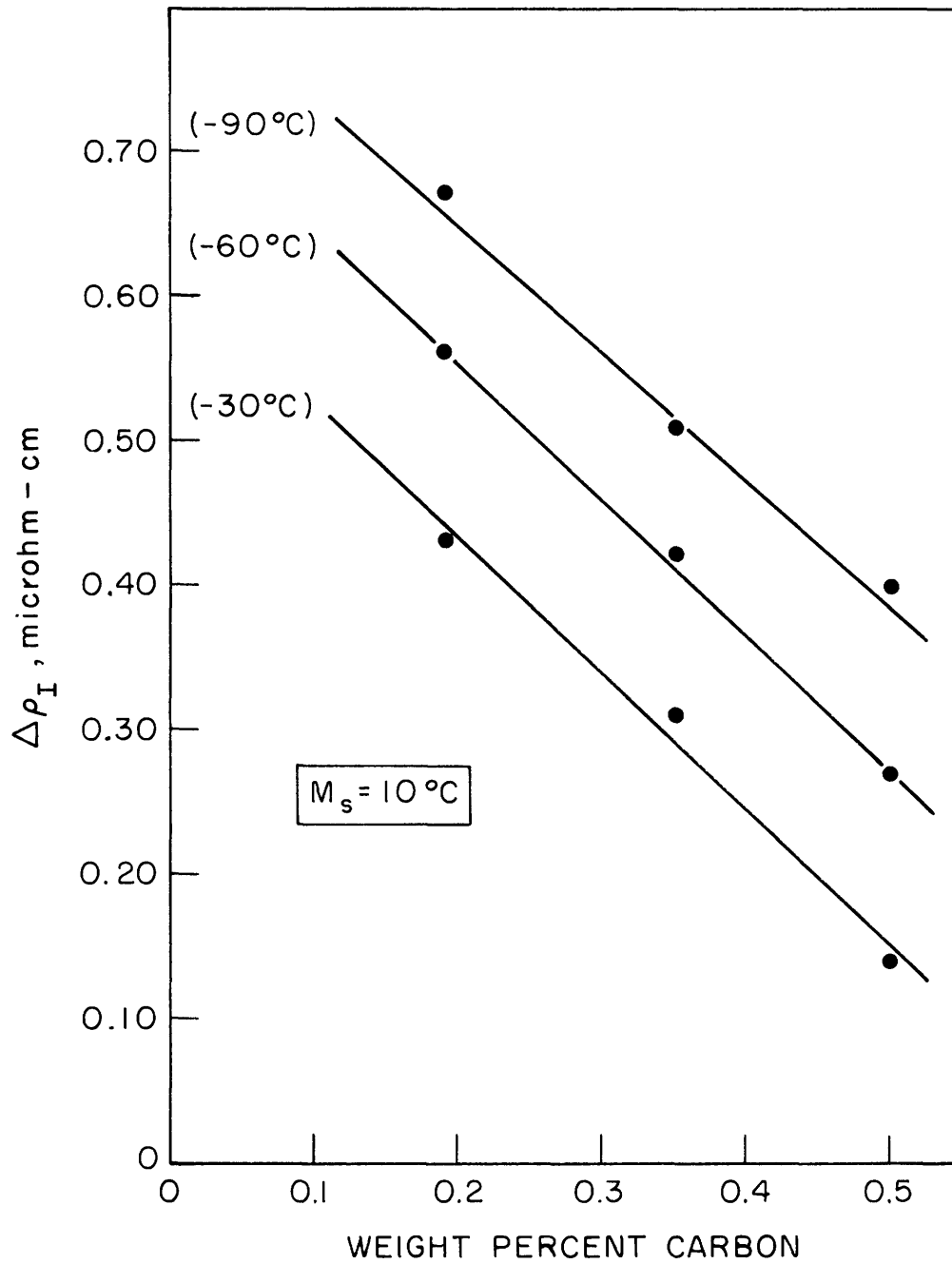
FIGURE 17. INITIAL RESISTIVITY DROP VS. CARBON
CONTENT FOR ALLOYS WITH A CONSTANT
M_s OF +10°C, AGED AT INDICATED
TEMPERATURES

this temperature range. Eldis suggested that $\Delta\rho_I$ may be due to some relaxation of the quenched-in dislocation structure of the martensite. He points out that the activation energy observed here is about the same as that found for some types of thermally activated dislocation movements. (78-80) Such relaxation should be inhibited by interstitial impurity atoms, so $\Delta\rho_I$ would be expected to decrease with increasing carbon content. Inasmuch as this is the case when alloys with the same M_s temperature are compared, and since no other more likely mechanism comes to mind, the dislocation relaxation hypothesis appears to be the most appropriate explanation for Region I.

5.3.4 Region-II Increase in Resistivity

Region II, a resistivity peak, occurs in specimens aged at temperatures from 0 to 70 °C. Aging at ~30 °C produces some increase in resistivity after long times. Specimens aged at 100 °C and above apparently pass the peak within 0.25 minutes of aging, because their resistivities decrease continuously with time. The height of the peak ($\Delta\rho_{II}$) increases with carbon and nickel content (Fig. 18). $\Delta\rho_{II}$ does not seem to vary is a systematic way with aging temperature, and appears to remain the same within 20 percent.

The activation energy of the process causing the peak was determined by application of equation 17 to plots
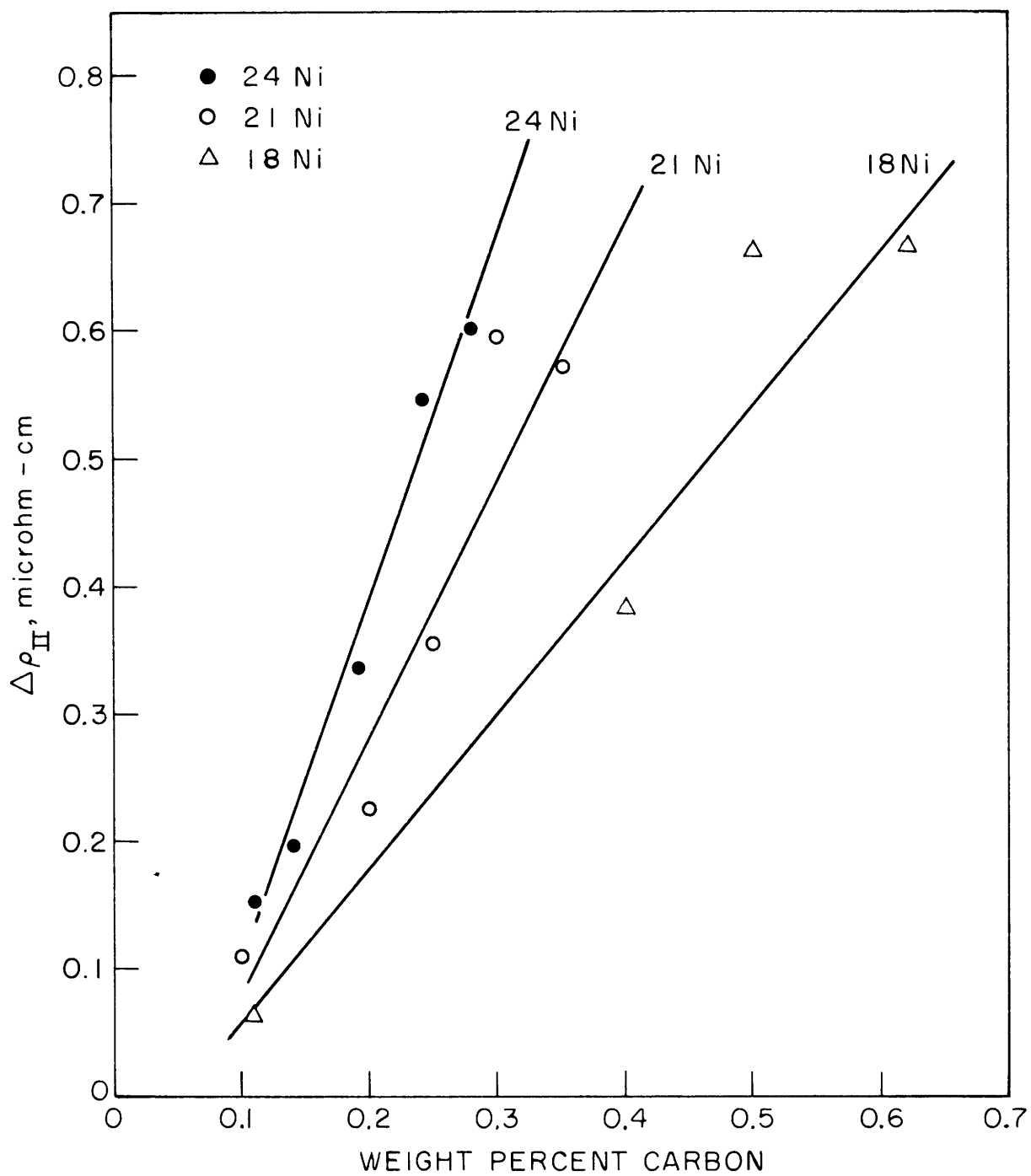
FIGURE 18. HEIGHT OF RESISTIVITY PEAK VS. CARBON CONTENT

of ln t vs. 1/T.* Values were determined at several
different points on both sides of the peak as well as at
the peak itself by assuming that, in samples aged at
different temperatures, the attainment of equal fractions
of total peak height corresponds to identical amounts
of the reaction. The activation energies thus obtained
vary from 18 kcal per mole during the early stages of the
increase, to 21 kcal per mole at the summit of the peak,
up to 24 kcal per mole during the decline. These values
were found to be the same for all the alloys.

In deciding what change in the martensite is
responsible for the resistivity peak, it is necessary to
consider the observations of other experimental methods
in the same time-temperature range. The x-ray diffraction
results discussed in Section 5.2 show that a low-
tetragonality martensite (α_t) forms during aging in this
temperature range. The activation energy for this process
is about 21 kcal per mole, which is in close agreement with
that for the resistivity peak. Furthermore, Hillert (77)
calculates the activation energy for carbon diffusion in
martensite to be:

$$Q_{mart.} = Q_{ferrite} + 3380X \qquad (21)$$

where X = weight percent carbon in the martensite
and $Q_{ferrite}$ = 20 kcal per mole (44)

*The data for $\Delta\rho_{II}$ were insufficient to apply equation 20.

Accordingly, for the carbon contents of interest, the measured Q values for the resistivity peak and for α_t formation are about the same as that for diffusion of carbon in martensite. Hence, the rate-controlling step in both cases appears to be carbon diffusion. On the basis of the x-ray results, the indications are that carbon atoms leave the octahedral sites occupied in virgin martensite and form carbon-rich clusters or find lower-energy sites at dislocations.

Electron microscopy has shown that micrographs of alloys aged in the temperature range of the resistivity peak have an unusaul mottled appearance and electron diffraction patterns exhibit distorted spots. Both these observations can be taken as evidence of carbon clustering in light of their similarity to observations on other systems known to form solute clusters.

In addition, Mössbauer measurements (50-51) strongly suggest that aging in this temperature range causes carbon-rich clusters to form. Choo and Kaplow (51) find that the structure of the clusters resembles that of Fe_4N, a face-centered cubic nitride observed by Jack (81) during the aging of iron-nitrogen martensite.

The Mössbauer, electron microscopic, and x-ray observations were made on martensites aged past the summit of the peak, where the resistivity begins to undergo a steady decrease.

Since (1) the activation energy for the peak agrees with that for diffusion of carbon, (2) no peak is observed in nil-carbon alloys, and (3) peak height increases with carbon content, it is clear that carbon movements are involved in the cause of the peak. Carbide precipitation may be ruled out as the source of the peak on the grounds that no carbides are observed to form until very much later in the aging. In the present case, carbides are first seen after aging for one hour at 150 °C, a condition much past the peak. The two other possible processes involving carbon are clustering and segregation to lower-energy sites, such as dislocations.

According to the previously discussed ideas about the origin of martensite resistivity, the increase in resistivity in Region II reflects an increase in the mean-square displacements, $\bar{\mu}^2$, of iron atoms from their equilibrium positions. If carbon segregation to dislocations does take place, the driving proce would be a reduction in elastic strain energy. The occupation of dislocation sites by carbons produces less distortion of the lattice than occupation of octahedral sites away from dislocations. This implies that $\bar{\mu}^2$ should decrease with such segregation and cause a <u>decrease</u> in resistivity. On the other hand, Hoffman (58) has shown that clustering may be considered to be a kind of spinodal decomposition

in which a decrease in elastic free energy is accompanied
by an increase in $\bar{\mu}^2$. Russian (60) investigators have
suggested that a spinodal-type of clustering reaction
is responsible for the distorted electron diffraction
spots observed during aging. The carbon-carbon binding
energies calculated by Johnson (53-54) imply that cluster
formation is energetically favorable. Wilkes (82) has
proposed a hypothesis which accounts for the resistivity
peak during early stages of G. P. zone formation, but is
generally applicable to any clustering system. He
postulates a stage, reached fairly early in zone formation,
when electron scattering is a maximum giving rise to a
peak in resistivity. This hypothesis fits very well with
the present observation that the resistivity peak occurs
early in the aging compared with the aging times required
to produce observable clustering effects in the x-ray,
Mössbauer and electron microscopy results. According
to Wilkes' suggestion, the resistivity decrease following
the peak is due to the clusters exceeding some optimum
scattering size. Similarly, in the Hoffman spinodal
proposal, though $\bar{\mu}^2$ continues to increase throughout the
clustering, the distribution of distortions becomes
concentrated in the immediate area of clusters so that
most of the atoms in the lattice are undisplaced. This
would lead to a resistivity decrease during later stages
of the process. Hence, the Wilkes and Hoffman proposals
accounting for the resistivity peak and subsequent decrease

are qualitatively alike.

Thus clustering of carbon atoms seems to account fully for the observed phenomena and we conclude that it is the cause of the resistivity peak and the beginning phase of the subsequent resistivity decrease. Dislocation segregation, to the extent that it may occur, must involve only a small fraction of the carbons present; otherwise the peak would not be measurable. Moreover, the 18 nickel-0.11 carbon alloy would exhibit no resistivity peak if such segregation predominated since the lath martensite in this alloy should have enough dislocations to provide sites for all the carbon atoms. (46)

5.3.5 Region-III Resistivity Decrease

After achieving the peak of Region II, the resistivities of the specimens decrease steadily. Since, as was concluded in the previous section, the resistivity peaks are found fairly early in cluster formation, the subsequent decrease encompasses almost all of the decomposition of martensite (eventually) into α-ferrite and cementite. For simplicity we may consider the start of the carbide-precipitation process (f=0) to be where the resistivity is equal to its initial as-quenched value after passing the peak. It is expected that the resistivity will decrease linearly with the amount of carbon removed from solution to form carbides, and we assume that the process of martensite decomposition is complete (f=1) when

the resistivity decline levels off or reaches a plateau on
aging at 300 or 350°C. This overall decrease in resistivity,
which increases with alloy carbon content, is then prorated
to indicated fraction transformed, as shown in the right-
hand scales of Fig. 13b-e. Thus, a basic assumption in
assigning values of f to points on resistivity curves is
that two specimens having equal normalized resistivity
changes after aging at different temperatures are at
identical stages in the overall precipitation reaction.

A closer look at the shapes of the resistivity
curves in Region III reveals that they can be divided into
three subregions on the basis of changes in slope. In the
first subregion, the resistivity decrease is a continuation
of the decline from the peak. The second subregion starts
when the fraction transformed is between 0.3 and 0.4; here
the resistivity vs. log time curves decrease in slope. In
most instances this change in slope is gradual, but some
of the curves exhibit a definite elbow or break point.
This second subregion lasts until f = 1, the completion of
decomposition. A third subregion occurs in some specimens
aged for long times at 300 or 350°C after the resistivity
curves have reached the f = 1 level.

Activation energies for various fractions
transformed were calculated using Hillert's method, equation
20, and the results are presented in plots of Q vs. fraction
transformed for each alloy in Fig. 19. The details of the
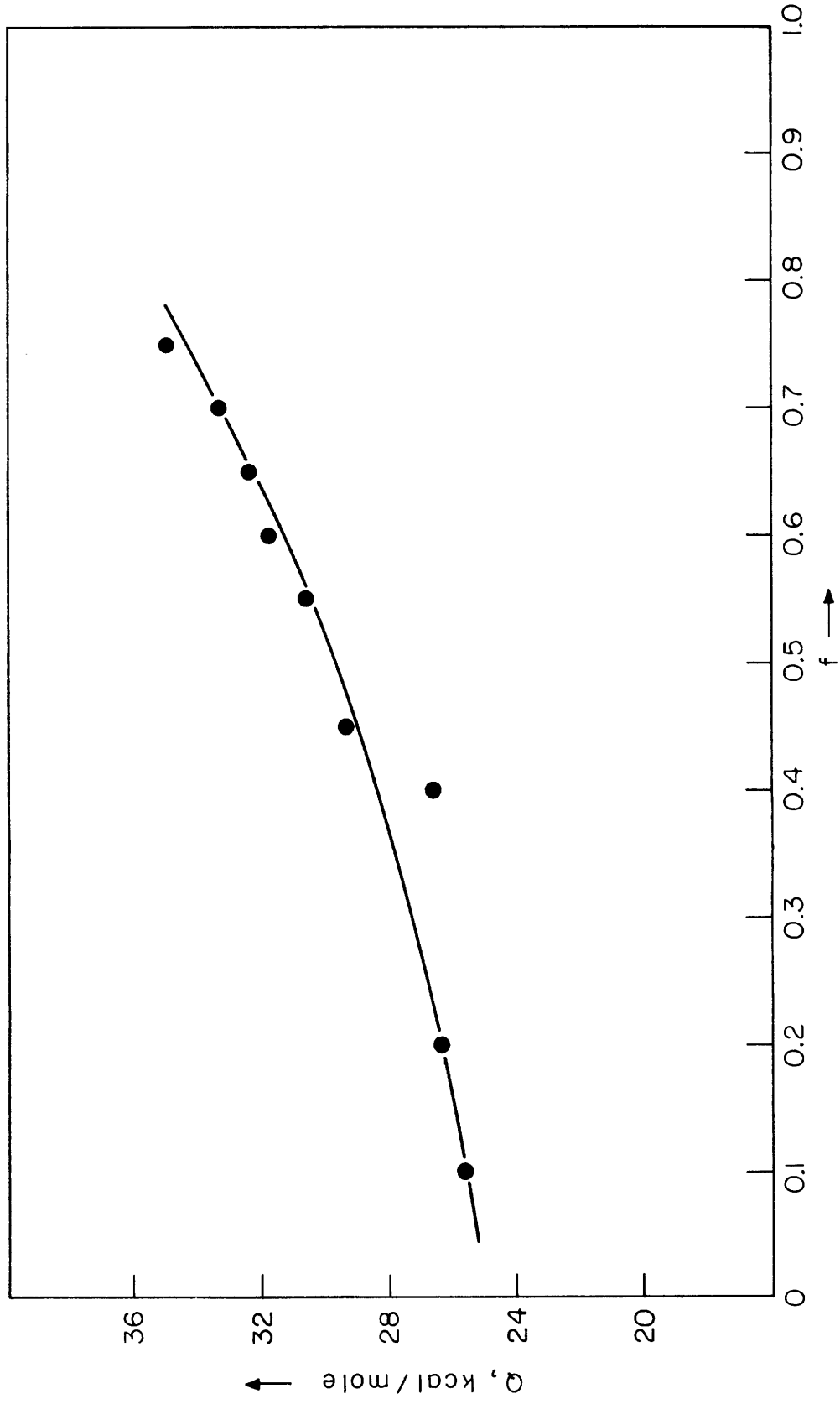
FIGURE 19a. ACTIVATION ENERGY VS. FRACTION TRANSFORMED FOR AN 18Ni-0.11C ALLOY
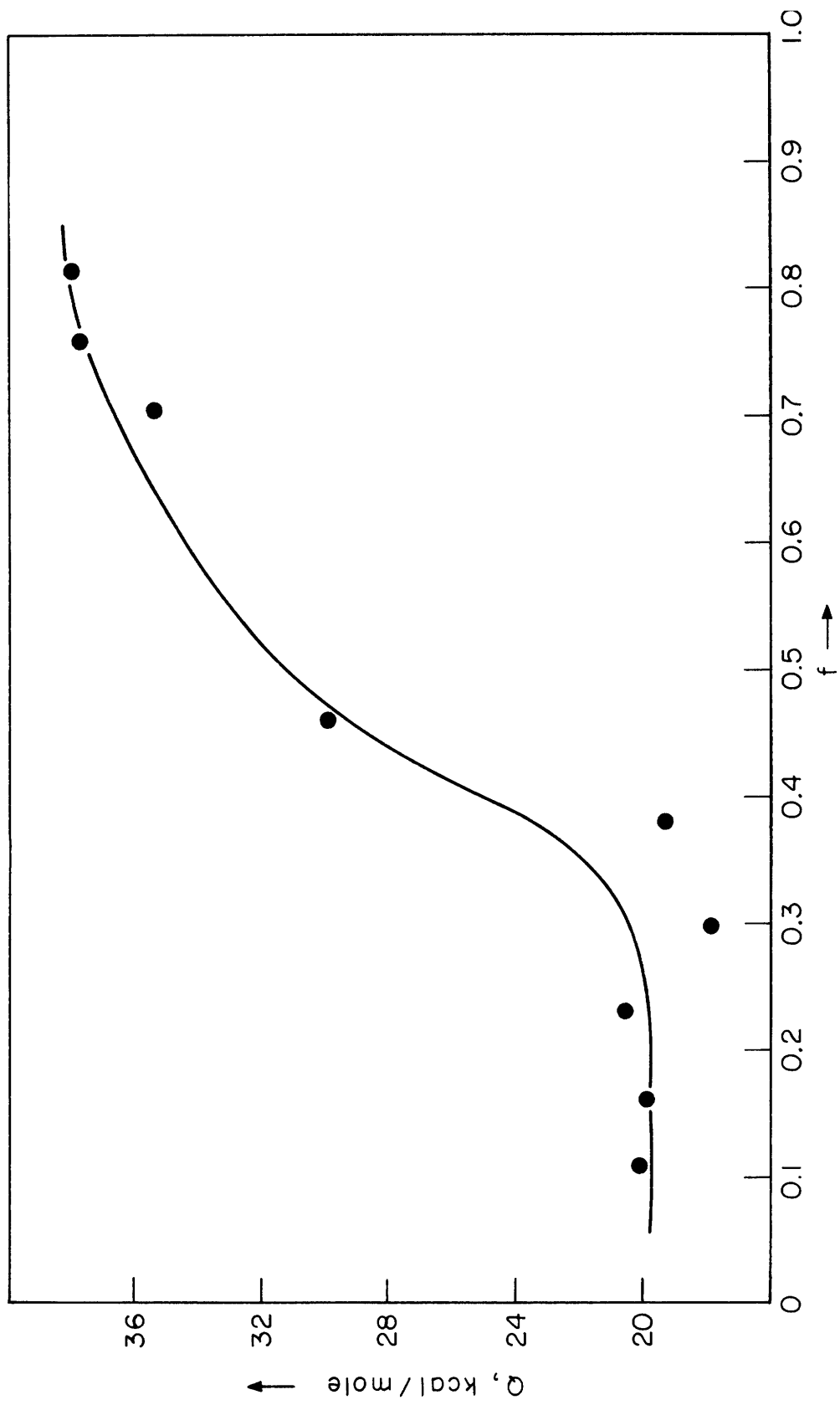
FIGURE 19b. ACTIVATION ENERGY VS. FRACTION TRANSFORMED FOR AN 18Ni-0.4C ALLOY
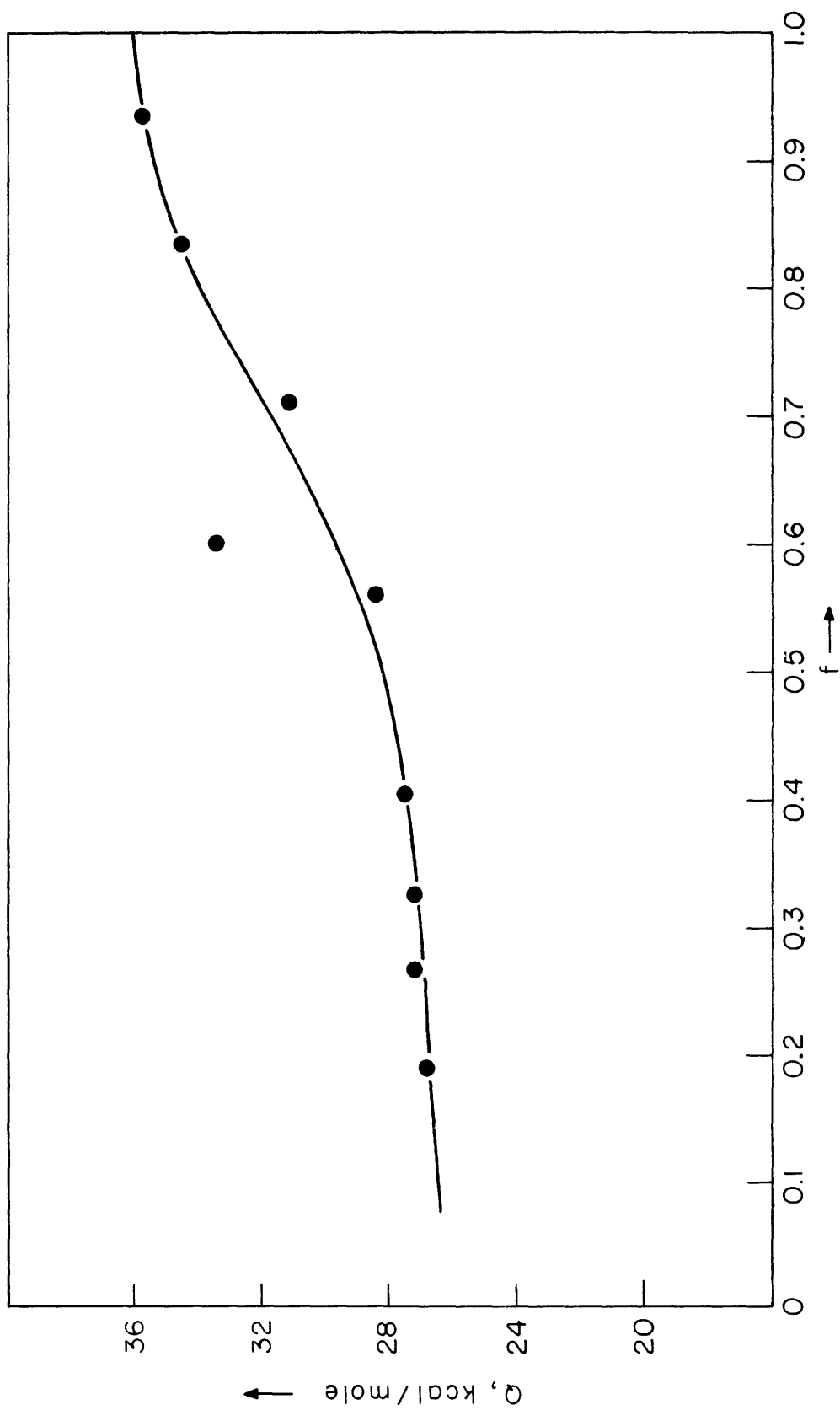
FIGURE 19c. ACTIVATION ENERGY VS. FRACTION TRANSFORMED FOR AN 18Ni-0.5C ALLOY

96
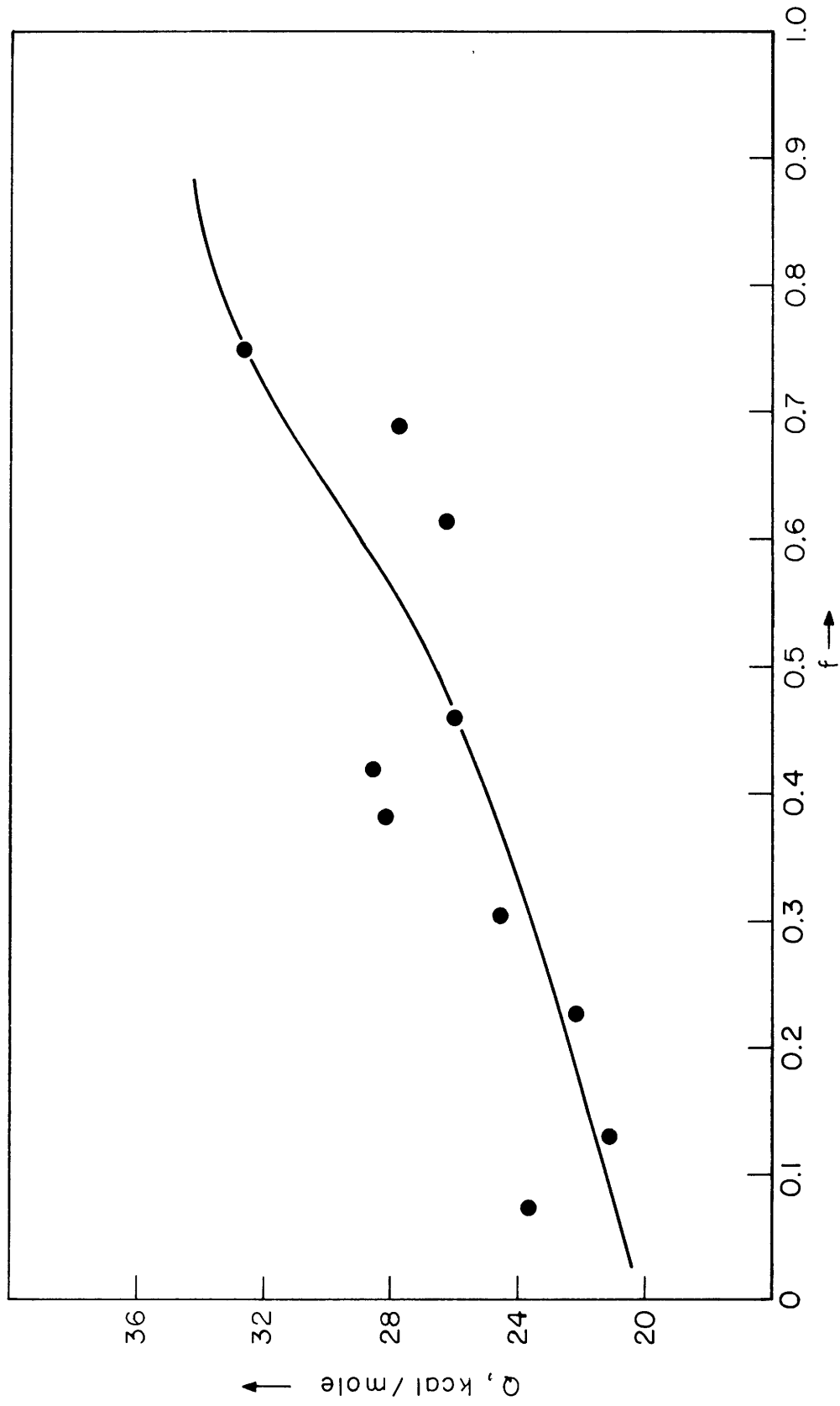
FIGURE 19d.   ACTIVATION ENERGY VS. FRACTION TRANSFORMED FOR AN 18Ni–0.62C ALLOY

curves differ somewhat, but this may be due, at least in part, to the procedures used to normalize the data (see section 5.3) rather than to any significant difference in behavior among the alloys. The results are in reasonable agreement with those of Kerlins and Altstetter (43) and Eldis (44).

The activation energy starts at values from 20 to 25 kcal per mole during the first 30 to 40 percent of the transformation. These values are consistent with those obtained for the resistivity peak and for α_t formation. Carbides can be detected by electron microscopy after three hours of aging at 100°C (45) or one hour at 150°C. This corresponds to a fraction transformed of about 0.4. Because of the similarity of activation energy, and because carbides are not yet precipitating in this first subregion of Region III we conclude that the initial part of the resistivity decline, up to about 40 percent transformation, is due to a continuation of the carbon clustering process responsible for the resistivity peak.

The activation-energy values begin to increase when the change of slope of the resistivity curves near $f = 0.4$ is reached. In those curves with no distinct elbows, the increase in Q begins at lower f levels and is more gradual, becoming in effect a continuous increase. Ultimately, the activation energy reaches a value between 33 and 37 kcal per mole when f is about 0.7. Since carbide

precipitation is first detected when f is about 0.4, we conclude that the increasing Q values correspond to some mixture of the activation energies of carbide precipitation and clustering. After 70 percent transformation, carbide precipitation is the predominant change occurring as reflected by the leveling off of the Q values at about 35 kcal per mole, which we take as the activation energy for carbide formation. There appears to be no pronounced difference in the activation energy for the formation of ε-carbide and for cementite. The value of 35 kcal per mole for carbide precipitation is in reasonable agreement with that reported by Eldis (44), who concluded, on the basis of similar activation energies, that the rate-controlling mechanism for carbide formation is pipe diffusion of iron atoms away from the growing carbides. The present data supports this conclusion. It is interesting to consider how the two types of carbides form. The Mössbauer, resistivity and electron-microscopy results indicate that most or all of the carbon atoms in martensite are grouped in the Fe_4C clusters at the time ε-carbide begins to appear. From the electron micrographs, it is seen that the ε-carbide forms as a finely dispersed network of thin particles. If, as has been suggested, the mottling in the micrographs of specimens tempered at lower temperatures is a manifestation of clustering, then it is possible that the clusters act as nuclei or preferred sites for the

ε-carbide. A scheme of precipitation can be envisioned
during which clusters of carbon atoms grow coherently to
some critical size, after which iron atoms diffuse away
by a pipe-diffusion mechanism. The remaining clusters
thus become richer in carbon, perhaps approaching the
$Fe_{2.4}C$ composition of ε-carbide. An accompanying loss
of coherency would then permit the hexagonal (or ortho-
rhombic) structure of ε-carbide to form. In this sense,
the clustering can be considered as a step in the formation
of ε-carbide analogous to the precipitation of θ' from
G. P. zones in the aluminum-copper system. On the other
hand it is also possible that ε-carbide nucleates in the
classical way with the clusters serving as heterogeneous
nucleation sites.

In contrast cementite appears to nucleate and
grow separately from the clusters or from the ε-carbide
particles. However, the rate-controlling step is evidently
the same as for ε-carbide precipitation, in that no
difference in activation energy can be detected.

In essence, the process of martensite decomposition
has two activation energies; one for the formation of
clusters where the rate-controlling step is carbon diffusion,
while the other is for carbide precipitation where the
mechanism is probably iron-pipe diffusion.

The final drop in resistivity of specimens aged
for prolonged periods at 300 and 350°C (the third subregion
of Region III) is probably not due to further carbide

precipitation, since the completion of precipitation is signaled by the leveling off of the resistivity curves, at which time the overall decrease in resistivity is commensurate with the total removal of carbon from solution in the martensite. Not enough data could be obtained to determine the activation energy for the third subregion but comparison of micrographs of specimens aged for 60 minutes and 10,000 minutes at 350°C suggests that recovery and recrystallization may be responsible (Fig. 9e,10e, and 20).
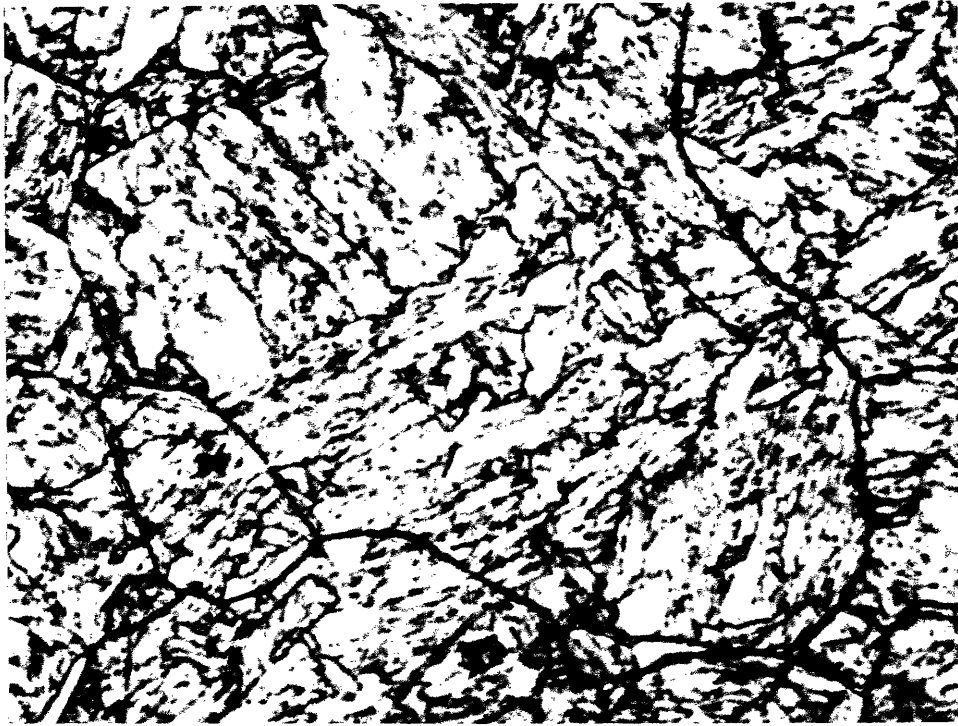
(a) 18Ni-0.11C Lath Martensite. 1000X

(b) 18Ni-0.4C Twinned Martensite. 1000X

Figure 20: Optical micrographs of martensite aged for
10,000 minutes at 350°C. Compare with
Fig. 7e and 8e. 1% Nital etch.

Chapter VI

SUMMARIZING DISCUSSION

6.1 The Structure of Virgin Martensite

The results of this and other studies have shown
that virgin twinned martensite is body-centered tetragonal
with the c/a ratio increasing linearly as a function of
carbon content. Although no similar direct observations
on the tetragonality of virgin lath martensite were
possible, due to the relatively high M_s temperatures, a
strong case can be developed to show that it, too, must
be tetragonal

The face-centered cubic austenite has one
octahedral site per iron atom, while the body-centered
martensite has three; each of a different orientation.
Thus, one of the consequences of the Bain distortion is
the tripling of octahedral sites. If there are carbons
present in the austenite and they do not jump from site
to site during the martensitic transformation, then all
the carbons will occupy one of the three sets of sites
in the body-centered phase causing it to be tetragonal.
This is the observed case in twinned martensite. Since
the resistivity results for lath and twinned martensites
are identical (except for the greater resistivity changes
in the twinned due to higher carbon contents), we may
infer that the difference in substructure of the two
types of martensite has relatively little effect on aging

behavior. Consequently, we may rule out segregation of carbon atoms to dislocations due to autotempering as a likely cause of the loss of tetragonality, since enough carbons remain in solution to form clusters in both types of martensite.

Another way for a nontetragonal martensite to form is by disordering of carbons such that the three sets of octahedral sites are equally populated. The occurrence of such disordering should be independent of the morphology, since the substructure does not enter into the disordering, the latter being accomplished by one or two atomic jumps. The activation energy of such a process would be about 21 kcal per mole, the same as that for cluster formation, inasmuch as the same rate-controlling step is involved. However, the total number of jumps necessary for disordering is much smaller than for clustering and so disordering should reach completion in a much shorter time.

Moreover, disordering should manifest itself by a gradual, rather than a discontinuous, decrease in the c/a ratio, and the lattice parameter of cubic, disordered martensite should be larger than that of nil-carbon iron because a hydrostatic dilatation of the lattice takes place when carbon atoms are in solution. (23) The changes observed by x-ray diffraction of twinned martensite exhibit neither a continuous decrease in c/a ratio not a hydrostatic dilatation of the lattice after the c/a drop. Hence, we may conclude that no disordering is observed in twinned

martensite.   In addition, because of the similar resistivity results for lath martensite, it appears that no disordering occurs in martensite of this morphology either.

The various interstitial ordering theories (31-35) predict that disordering of carbon atoms takes place only when the temperature of the martensite is above a critical temperature which is proportional to the carbon content of the martensite. A discussion of the theories is presented in the Appendix.   On this basis, the twinned martensites might all form below their ordering temperatures and so be tetragonal, while the lath martensites might be cubic because of formation above their ordering temperatures. However, the theories predict that the critical temperature for ordering is about 1000 times the weight percent carbon in the alloy, while a slope more than sixty times as large would be needed to account for all the observations of tetragonality in virgin martensite (Fig. 21).   Thus, the ordering theories are not successful at predicting tetragonality in virgin twinned martensite, and the same should hold true for the case of lath martensites.

We come to the conclusion that the structures of both twinned and lath virgin martensite are body-centered tetragonal, and any observations to the contrary are probably due to autotempering of carbons to form clusters and/or the inability of most conventional diffraction techniques to detect a closely spaced tetragonal doublet.
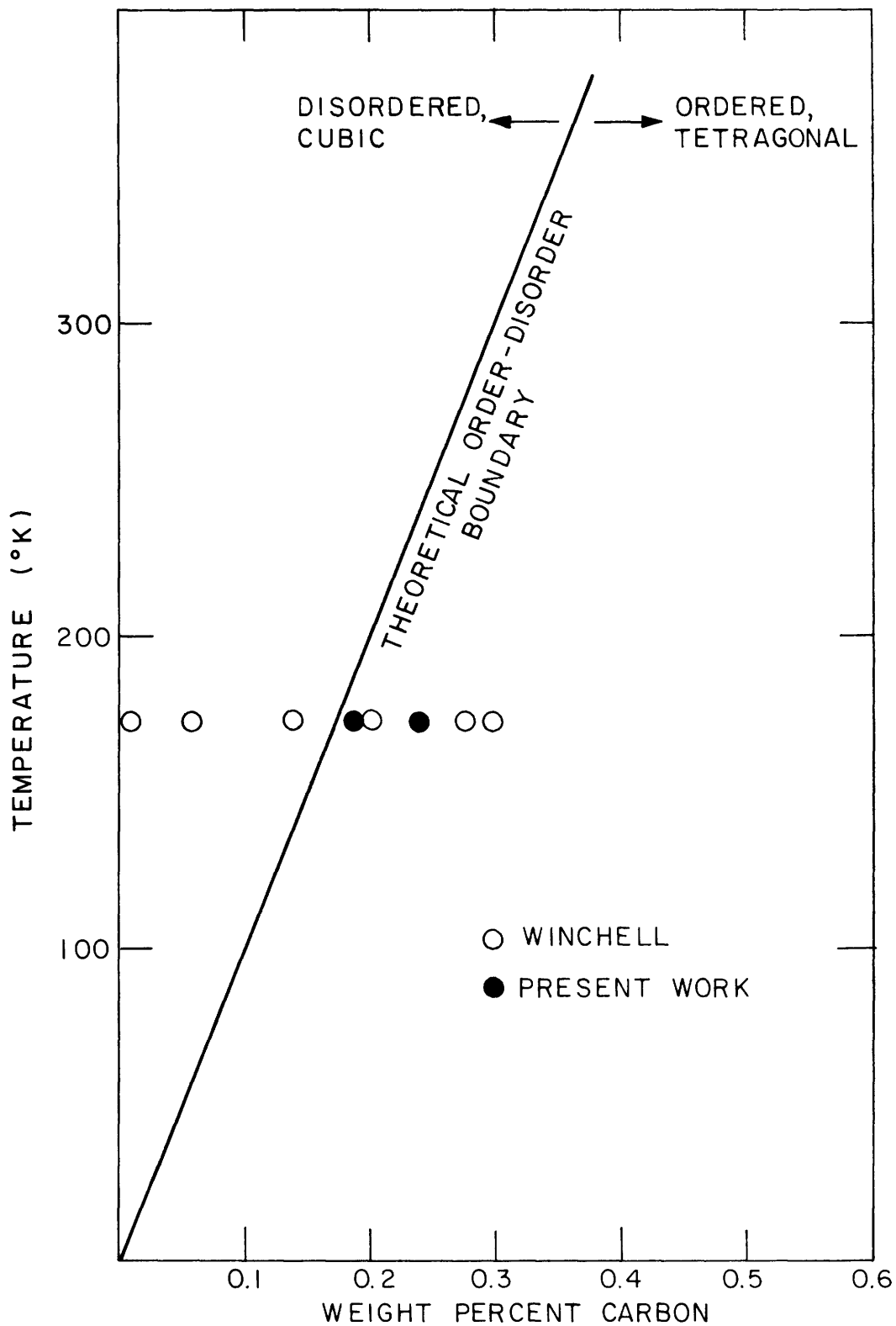
FIGURE 21 CRITICAL TEMPERATURE FOR ORDERING VS
CARBON CONTENT SHOWING COMPOSITIONS
AND TEMPERATURES WHERE TETRAGONAL
MARTENSITE HAS BEEN OBSERVED

6.2 The Aging of Martensite

The results of this research have shown that both lath and twinned martensites undergo very similar changes during aging. The differences in substructural morphologies apparently have little effect on tempering behavior, because the carbon atoms cluster more rapidly than they can segregate to dislocation sites. This does not mean that dislocation segregation does not occur, merely that it is less important than cluster formation in the early aging of tetragonal martensites.

The long-standing division of the tempering of martensite into three stages can now be modified to include more detailed descriptions of each stage. An initial stage is added to include the low-temperature dislocation relaxation. The revised stages of tempering are presented in Table 2.

Table 2

THE STAGES OF TEMPERING

Stage	Type of Change	Temperature Range	Q (kcal/mole)
0th	Dislocation Relaxation	below room temperature	3
1st	Clustering, $\alpha' \to \alpha_t$	-30 to 100°C	21
	$\alpha' \to \alpha_t$ immediately followed by precipitation of ε-carbide	above 100°C	21 increasing to 35
2nd	Isothermal conversion of retained austenite (not observed in these experiments)	above 200°C	
3rd	Precipitation of ε-carbide and cementite, followed by resolution of the ε leading to the equilibrium mixture of α-Fe and cementite	above 200°C	35
	Recovery and recrystallization	above 300°C	

Chapter VII
CONCLUSIONS

1. The virgin structures of both lath and twinned martensite are body-centered tetragonal with a c/a ratio increasing with carbon content according to:

$$c/a = 1.005 + 0.057(w/o\ C)$$

2. While the substructures of the two martensitic morphologies are quite different, both exhibit very similar behavior during aging.

3. The changes during the aging of virgin martensite can be divided into the following overlapping steps:

   a) Dislocation relaxations occur during aging below room temperature. The activation energy for such relaxations is about 3 kcal per mole.

   b) The formation of carbon clusters (of approximate composition Fe_4C) takes place when martensite is aged at temperatures from -30 to +200°C. The rate-controlling process for such clustering is the diffusion of carbon interstitials in martensite with an activation energy of 21 kcal per mole.

c) ε-carbide particles precipitate during aging above 100°C; the corresponding activation energy is about 35 kcal per mole suggesting that the rate-controlling process is pipe diffusion of iron atoms away from the growing carbide particles. There are strong indications that the carbon clusters formed earlier are a precursor to the ε-carbide precipitation.

d) Cementite particles nucleate and grow at aging temperatures above 200°C. The activation energy is the same as that for ε-carbide formation, suggesting that the same rate-controlling process is at play in both instances.

e) Recovery and recrystallization occur when martensite is aged at temperatures above 300°C.

4. Interstitial ordering theories are not successful in predicting whether or not virgin martensite is tetragonal or cubic. There is no evidence that disordering of carbon atoms takes place to cause the formation of body-centered cubic martensite.

Chapter VIII

SUGGESTIONS FOR FURTHER WORK

1. The tetragonality of virgin lath martensite has still not been determined by direct observation. Perhaps closer-spaced compositions or more sophisticated specimen preparation could allow the pseudo-single crystal method to be used for such measurements.

2. The nature of the carbon clustering during the early stages of aging should be more fully explored. This can be done by a combination of x-ray, electron microscopy and Mössbauer experiments. It would be desirable to show more definitely whether ε-carbide nucleates heterogeneously near the clusters and grows at their expense or whether the clusters themselves gradually develop into ε-carbide. Also of interest is the 1.004 axial ratio of α_t, and its relation to the clusters. The exact cause of this low tetragonality during aging remains to be established.

3. More accurate values for the activation energy of each step of aging could be obtained by additional resistivity runs at smaller temperature intervals. Combined with structural observations, this information could lead to a more detailed understanding of the mechanisms of tempering. Furthermore, such resistivity data could lead

to an improved theory of the resistivity of clustered and multiphase alloys.

4. The theories of martensite strengthening should be re-examined in the light of the clustering stage of aging.

5. Experiments with very high-carbon alloys would be of interest because the structure of martensite and the phenomena of aging should be easier to observe in such alloys than in alloys with less carbon.

APPENDIX

Application of Interstitial Ordering Theories

to Fe-Ni Alloys

The theories concerning interstitial ordering
reactions (31-35) were originally developed for the case
of carbon atoms in solution in pure body-centered iron.
However, the experimental data in this thesis available
to test the applicability of these theories were for
Fe-Ni alloys containing between 20 and 30 weight percent
nickel. Consequently, it was necessary to take the
addition of nickel into account in the ensuing calculations.

The calculations of the critical temperature
for interstitial ordering in all theories can be affected
by the addition of nickel to the alloy in two ways: 1) The
lattice parameters of Fe-Ni alloys decrease as nickel content
increases, in the nickel range of interest, thus requiring
larger distortions of the lattice to accommodate carbon
interstitials, and 2) the elastic constants of Fe-Ni alloys
decrease as nickel content increases, thus making it easier
for carbon atoms to expand the lattice. Clearly, these
effects work in opposing directions. However, the elastic
constants drop by as much as 35 percent in going from zero
to 30 percent nickel (76) while the variation in lattice
parameter is only a tenth as much. (72) Therefore, only

the change in elastic constants was considered in the
calculations to be discussed here.

To obtain the Fe-Ni elastic constants of interest,
values for the bulk elastic constants E (Youngs Modulus)
and G (shear modulus) for α-phase alloys were obtained
from Marsh (76). Then, using the Reuss averaging
expressions for bulk elastic constants and J = 0.601
(the compliance anisotropy factor for pure iron) (83)
the elastic compliances and constants were calculated.
It was assumed that the elastic anisotropy of Fe-Ni alloys
is the same as that of pure Fe. The elastic constants
obtained are listed in Table A1.

1. Polder (32) considers the contribution to
the free energy of the strain energy produced by
distributions of carbons among the three sets of octahedral
sites, and concludes that in the absence of applied stress,
carbon atoms will populate all three sets of sites equally.
This means no critical temperature for ordering exists because
tetragonal martensite is not considered to be thermo-
dynamically stable. Polder suggests that the reason carbon
atoms in tetragonal martensite remain ordered at room
temperature may be due to a much slower diffusion of carbon
in martensite than in α-Fe.

2. Zener (31) has derived an interstitial ordering
theory based on the energy change associated with moving a
carbon atom from a disordered to an ordered site, the strain

Table A2

ELASTIC CONSTANTS OF BCC Fe-Ni ALLOYS

Constant	Pure Fe	Fe-20Ni	Fe-30Ni
E	2.08^*	1.72^*	1.52^*
G	0.81^*	0.67^*	0.59^*
s_{11}	0.760†	0.821√	0.898√
s_{12}	-0.287†	-0.289√	-0.311√
s_{44}	0.893†	1.010√	1.215√
c_{11}	2.42†	1.974√	1.761√
c_{12}	1.465†	1.072√	0.931√
c_{44}	1.12†	0.99√	0.85√

all units are 10^{12} dynes/cm² except s_{11}, s_{12} and s_{44} which are in 10^{-12} cm²/dyne

* Marsh (76)

† Hirth and Lothe (83)

√ calculated

energy produced by the expansion of the lattice, and the
variation in entropy with the degree of interstitial
order. A critical temperature is predicted because at low
temperatures the entropy contribution to free energy (G)
is small and so G is minimized when the atom configuration
with the lowest combination of chemical and strain energies
is achieved. At higher temperatures the entropy term
predominates and the disordered configuration of atoms
posses the lowest free energy. The Zener prediction of
the critical temperature is:

$$T_c = 0.243NE_{100}\lambda^2/k \qquad\qquad (A1)$$

in which $N = 3.92 \times 10^{21}$ (w/o C), the number of carbon atoms
    per unit volume

$E_{100} = 1/s_{11}$, Youngs Modulus in the [100] direction

$\lambda = 1.2 \times 10^{-23}$, the strain of transferring one
    carbon per unit volume from a disordered to
    an ordered site

k = Boltzmann's constant

3. The Fisher theory (33) is derived by computing
the elastic energy of an interstitial atom through a
detailed consideration of the displacements of the 32 iron
atoms nearest to a carbon interstitial. An expression for
the free energy is developed, and conditions for its minimum
are derived from which an equation for the critical

temperature for ordering is obtained:

$$T_c = \frac{n(f_1 a^2 e_0)^2}{12k(c_{11}-c_{12})} \qquad (A2)$$

where n = number of interstitials per cm^3

$a = 2.866 \times 10^{-8}$ cm, the lattice parameter of iron

$e_0 = 0.19$, the dipole strain of an interstitial estimated from the tetragonal lattice parameters of martensite

k = Boltzmann's constant

c_{11}, c_{12} = elastic constants

f_1 = force on the two nearest-neighbor iron atoms necessary to maintain equivalent distortion of an interstitial; this is a function of both the elastic constants and the displacements of the 32 irons surrounding the interstitial site

4. The treatment of interstitial ordering by Nowick and Heller (34) considers the interactions of the distortion dipoles of occupied interstitial sites. The underlying idea is that as the concentration of interstitials is increased, mutual interactions lead to the ordered configuration having the lowest free energy. The critical temperature predicted by this theory is:

$$T_c = \frac{c_0 v_0 (\lambda_1 - \lambda_2)^2 (c_{11} - c_{12})}{3k} \qquad (A3)$$

in which c_0 = mole fraction of interstitials

$v_0 = a^3/2 = (2.866 \times 10^{-8})^3/2$ = molecular volume

c_{11}, c_{12} = elastic constants

k = Boltzmann's constant

$(\lambda_1 - \lambda_2)$ = 1.06, obtained from anelastic

measurements on single crystals, where λ_1 and λ_2

describe the strain around the interstitial site

5. Khachaturyan (35) derived his interstitial
ordering theory from a treatment of the elastic interactions
of pairs of interstitials, an approach similar to that of
Nowick and Heller. The expression for the critical
temperature is:

$$T_c = \frac{c(3-c)}{9(1-c)^2} \frac{v}{k} \frac{(c_{11}-c_{12})^2 (\gamma_1 - \gamma_2)^2}{c_{11}-c_{12}+c_{44}} \qquad (A4)$$

in which c = atom fraction of carbons

v = molecular volume of iron

k = Boltzmann's constant

c_{11}, c_{12}, c_{44} = elastic constants

γ_1 = -0.117

γ_2 = 0.917, representing the rate of change of

the a and c lattice parameters, respectively,

with the addition of carbon

The critical temperatures as recalculated
using the elastic constants listed in Table A1 are presented
in Table A2. It is evident that the predictions of the
various theories are quite similar. It is difficult to
decide which approach is on the firmest theoretical
grounds. However, all of the theories contain the
obviously invalid assumption that linear elasticity holds
true for the very large distortions around interstitial
carbon atoms. A more serious short-coming is that these
order-disorder theories are all refuted by the available
lattice-parameter measurements which clearly show (Fig. 21)
that Fe-Ni-C martensites remain tetragonal at temperatures
well above critical temperatures deduced from Table A2.

Table A2

CRITICAL TEMPERATURES FOR CARBON ORDERING

$$T_c \ ^\circ K = M(w/o \ C) \qquad (M \ values \ are \ tabulated)$$

Theory	Fe	Fe-20Ni	Fe-30Ni
Zener	1298	1204	1098
Fisher	823	744	572
Nowick and Heller	1413	1335	1224
Khachaturyan	1165	1140	1081

BIBLIOGRAPHY

1.   B. A. Rogers, The Nature of Metals, MIT Press,
      Cambridge, Mass. (1953) 3 and 129.

2.   M. Cohen, "The Strengthening of Steel", Trans. AIME
      224 (1962) 638.

3.   D. P. Antia, S. G. Fletcher and M. Cohen, "Structural
      Changes During the Tempering of High Carbon Steel",
      Trans. ASM 32 (1944) 290.

4.   S. G. Fletcher and M. Cohen, "The Effect of Carbon on
      the Tempering of Steel", Trans. ASM 32 (1944) 333.

5.   R. F. Bunshah and R. F. Mehl, "Rate of Propagation
      of Martensite", Trans. AIME 197 (1953) 1251.

6.   L. Kaufman and M. Cohen, "Thermodynamics and Kinetics
      of Martensitic Transformations", Progress in Metal
      Physics 7 (1958) 165.

7.   P. Clapp, Discussion of martensite nucleation at
      Boston Chapter AIME January 1972 meeting.

8.   L. Kaufman, "Current Assessment of the Thermodynamics,
      Structure and Nucleation of Ferrous Martensite",
      presented at the International Symposium on Metallurgical
      Chemistry "Applications in Ferrous Metallurgy"
      July 19-21, 1971, University of Sheffield, Sheffield,
      England (held under BISRA auspices).

9.   D. P. Dunne and C. M. Wayman, "The Crystallography of
      Ferrous Martensites", Met. Trans. 2 (1971) 2327.

10. P. M. Kelly and J. Nutting, "The Morphology of Martensite", Journal Iron and Steel Institute 197 (1961) 199.

11. R. L. Patterson and C. M. Wayman, "Internal Twinning in Ferrous Martensites", Acta Met. 12 (1964) 1306.

12. G. R. Speich and P. R. Swann, "Yield Strength and Transformation Substructure of Quenched Iron-Nickel Alloys", Journal Iron and Steel Institute 203 (1965) 480.

13. A. R. Marder and G. Krauss, "The Morphology of Martensite in Iron-Carbon Alloys", Trans. ASM 60 (1967) 651.

14. J. R. Mihalisin, "Effect of Carbon Content on Transformation Structures of Iron 22 percent Nickel Alloys", ASTM STP430 (1960) 250.

15. G. Krauss and A. R. Marder, "The Morphology of Martensite in Iron Alloys", Met. Trans. 2 (1971) 2343.

16. O. Johari and G. Thomas, "Factors Determining Twinning in Martensite", Acta Met. 13 (1965) 1211.

17. K. Shimizu and C. M. Wayman, "Discussion of 'Factors Determining Twinning in Martensite'", Acta Met. 14 (1966) 1390.

18. O. Johari and G. Thomas, "Reply to 'Discussion of 'Factors Determining Twinning in Martensite''", Acta Met. 14 (1966) 1392.

19. R. F. Vyhnal and S. V. Radcliffe, "Effect of Pressure on the Structure of Iron-Carbon Martensites", Acta Met. 15 (1967) 1475.

20. R. G. Davies and C. L. Magee, "Austenite Ferromag-netism and Martensite Morphology", Met. Trans. 1 (1970) 2927.

21. R. G. Davies and C. L. Magee, "Influence of Austenite and Martensite Strength on Martensite Morphology", Met. Trans. 2 (1971) 1939.

22. P. G. Winchell, The Structure and Mechanical Properties of Iron-Nickel-Carbon Martensites, PhD Thesis, MIT (1958).

23. E. J. Fasiska and H. Wagenblast, "Dilation of Alpha-Iron by Carbon", Trans. AIME 239 (1967) 1818.

24. D. T. Keating and A. N. Goland, "Atomic Displacements in Martensite", Acta Met. 15 (1967) 1805.

25. S. C. Moss, "Static Atomic Displacements in Iron-Carbon Martensite", Acta Met. 15 (1967) 1815.

26. J. C. Swartz, J. W. Shilling and A. J. Schwoeble, "Dipolar Strains of C and N in Alpha-Iron", Acta Met. 16 (1970) 1359.

27. P. G. Winchell and G. R. Speich, "Point Defect Supported Martensite Tetragonality", Acta Met. 18 (1970) 53.

28. C. S. Roberts, "Effect of Carbon on the Volume Fractions and Lattice Parameters of Retained Austenite and Martensite", Trans. 197 (1953) 203.

29. F. E. Werner, B. L. Averbach and M. Cohen, "The Tempering of Iron-Carbon Martensite Crystals", Trans. ASM 49 (1957) 823.

30. P. G. Winchell and M. Cohen, "The Strength of Martensite", Trans. ASM 55 (1962) 347.

31. C. Zener, "Kinetics of the Decomposition of Austenite", Trans. AIME 167 (1946) 550.

32. D. Polder, "Theory of the Elastic After-Effect and the Diffusion of Carbon in Alpha-Iron", Phillips Research Reports 1 (1945) 5.

33. J. C. Fisher, "Elastic Interaction of Interstitial Atoms in Body Centered Cubic Crystals", Acta Met. 6 (1958) 13.

34. A. S. Nowick and W. R. Heller, "Anelasticity and Stress-induced Ordering of Point Defects in Crystals", Advances in Physics 12 (1963) 251.

35. A. G. Khachaturyan, "Some Aspects of the Microscopic Theory of Interstitial Tetragonal Solutions", Soviet Physics-Doklady 10 (1966) 1118.

36. W. S. Owen, E. A. Wilson and T. Bell, High-Strength Materials, ed. V. F. Zackay, John Wiley, N. Y. (1965) 167.

37. J. K. Stanley, "The Diffusion and Solubility of Carbon in Alpha-Iron", Trans. AIME 185 (1949) 752.

38. C. S. Roberts, B. L. Averbach and M. Cohen, "The Mechanism and Kinetics of the First Stage of Tempering", Trans. ASM 45 (1953) 576.

39.   B. S. Lement, B. L. Averbach and M. Cohen,
       "Microstructural Changes on Tempering Iron-Carbon
       Alloys", Trans. ASM 46 (1954) 851.

40.   B. S. Lement, B. L. Averbach and M. Cohen,
       "Further Study of Microstructural Changes on
       Tempering Iron-Carbon Alloys",Trans. ASM 47 (1955) 291.

41.   K. H. Jack, "Structural Transformations in the
       Tempering of High-Carbon Martensitic Steels", Journal
       Iron and Steel Institute 169 (1951) 26.

42.   M. G. H. Wells, "An Electron Transmission Study of the
       Tempering of Martensite in an Fe-Ni-C Alloy",
       Acta Met. 12 (1964) 389.

43.   V. Kerlins and C. Altstetter, "Kinetics of the Initial
       Stages of Decomposition of Low M_s Iron-Nickel-Carbon
       Martensites", Trans. AIME 227 (1963) 94.

44.   G. Eldis, Ausforming and Tempering of High-Alloy Steels,
       PhD Thesis, MIT (1971).

45.   D. W. Hoffman, Ausform-Strengthening of Iron-Nickel-
       Carbon Martensite, PhD Thesis, MIT (1966).

46.   D. Kalish and M. Cohen, "Structural Changes and
       Strengthening in the Strain Tempering of Martensite",
       Materials Science and Engineering 6 (1970) 156.

47.   C. J. Barton, "The Tempering of a Low-Carbon Internally
       Twinned Martensite", Acta Met. 17 (1969) 1085.

48.   Y. Hirotsu and S. Nagakura, "Crystal Structure and
      Morphology of the Carbide Precipitated from
      Martensitic High Carbon Steel During the First
      Stage of Tempering", Acta Met. 20 (1972) 645.

49.   G. R. Speich, "Tempering of Low-Carbon Martensite",
      Trans. AIME 245 (1969) 2553.

50.   J. R. Genin and P. A. Flinn, "Mössbauer Effect Study
      of the Clustering of Carbon Atoms During the Room
      Temperature Aging of Iron-Carbon Martensite",
      Trans. AIME 242 (1968) 1419.

51.   W. K. Choo and R. Kaplow, "Mössbauer Measurements
      on the Aging of Iron Carbon Martensite", (1972),
      to be published.

52.   V. I. Izotov and L. M. Utevskiy, "Structure of the
      Martensite Crystals of High Carbon Steel", Physics of
      Metals and Metallography 25 (1968) 86.

53.   R. A. Johnson, G. J. Diennes and A. C. Damask,
      "Calculation of the Energy and Migration Characteristics
      of Carbon and Nitrogen in α-Iron and Vanadium",
      Acta Met. 12 (1964) 1215.

54.   R. A. Johnson, "Calculation of the Energy and
      Migration Characteristics of Carbon in Martensite",
      Acta Met. 13 (1965) 1259.

55.   A. G. Khachaturyan, "Determination of the Energy of
      Elastic Interaction of Pairs of Impurity Atoms in a
      Crystal Lattice", Soviet Physics-Solid State 4 (1963)
      2081.

56.   A. G. Khachaturyan, "The Theory of the Tetragonality
      of Interstitial Solutions in B.C.C. Lattices", Fiz.
      Metal Metalloved 19 (1965) 343.

57.   D. W. Hoffman, "Concerning the Elastic Free Energy
      of Dilute Interstitial Alloys", Acta Met. 18 (1970) 819.

58.   D. W. Hoffman, privare communication.

59.   B. S. Lement and M. Cohen, "A Dislocation-attraction
      Model for the First Stage of Tempering", Acta Met.
      4 (1956) 469.

60.   G. V. Kurdjumov and A. G. Khachaturyan, "Phenomena
      of Carbon Atom Redistribution in Martensite", Met.
      Trans. 3 (1972) 1069.

61.   G. V. Kurdjumov and G. Sachs, "Über den Mechanismus
      der Stahlhärtung", Zeitschrift Für Physik 64 (1930) 325.

62.   F. E. Werner, Tempering of Iron-Carbon Single Crystals,
      PhD Thesis, MIT (1955).

63.   C. S. Roberts, Tempering Process in Iron-Carbon Alloys,
      PhD Thesis, MIT (1952).

64.   C. Barrett and T. B. Massalski, Structure of Metals,
      3rd Ed. McGraw-Hill, N. Y. (1966) 520.

65.   G. R. Speich, private communication.

66.   E. Tekin and P. M. Kelley, "A Study of the Tempering
      of Steel Using Transmission Electron Microscopy",
      Precipitation from Iron Base Alloys G. R. Speich and
      J. B. Clark eds. Gordon and Breach, N. Y. (1965).

67. L. E. Tanner, "Diffraction Contrast from Elastic
     Shear Strains due to Coherent Phases", Phil. Mag.
     14 (1966) 111.

68. P. J. Fillingham, H. J. Leamy and L. E. Tanner,
     "Simulation of Electron Transmission Images of
     Crystals Containing Random and Periodic Arrays
     of Coherency Strain Centers", Electron Microscopy and
     Structure of Materials, G. Thomas, ed. Univ. of
     Calif. Press, Berkeley (1972) 163.

69. P. E. Champness and G. W. Lorimer, "Electron
     Microscopic Studies of Some Lunar and Terrestrial
     Pyroxenes", Electron Microscopy and Structure of
     Materials, G. Thomas, ed. Univ. of Calif. Press,
     Berkeley (1972) 1245.

70. L. E. Tanner, "The Ordering Transformation in Ni_2V",
     to be published in Acta Met.

71. L. E. Tanner, private communication.

72. L. Zwell, D. E. Carnahan and G. R. Speich, "Lattice
     Parameter of Ferritic and Martensitic Fe-Ni Alloys",
     Met. Trans. 1 (1970) 1007.

73. J. K. Stanley, Electrical and Magnetic Properties of
     Metals, American Society for Metals, Metals Park,
     Ohio, (1963).

74. R. M. Bozorth, Ferromagnetism, D. Van Nostrand, N. Y.
     (1951) 104.

75. F. X. Kayser, private communication.

76. J. S. Marsh, The Alloys of Iron and Nickel,
     McGraw-Hill, N. Y. (1938).

77. M. Hillert, "The Kinetics of the First Stage of
     Tempering", Acta Met. 7 (1959) 653.

78. H. Conrad, "On the Mechanism of Yielding and Flow
     in Iron", Journal Iron and Steel Institute 198 (1961)
     364.

79. H. G. Van Bueren, Imperfections in Crystals,
     North-Holland Publishing Co. Amsterdam (1960).

80. A. Seeger and B. Šesták, "Microstrain and Dislocation
     Relaxations in BCC Metals", Scripta Met. 5 (1971) 875.

81. K. H. Jack, "The Occurrence and the Crystal Structure
     of α''-Iron Nitride; a New Type of Interstitial Alloy
     Formed During the Tempering of Nitrogen-Martensite"
     Proc. Roy. Soc. A208 (1951) 216.

82. P. Wilkes, "On the Anomalous Electrical Resistance
     of G. P. Zones", Acta Met. 16 (1968) 863.

83. J. P. Hirth and J. Lothe, Theory of Dislocations,
     McGraw-Hill, N. Y. (1968) 405 and 762.

BIOGRAPHICAL NOTE

Andrew Michael Sherman was born in Cleveland, Ohio on October 28, 1945. He attended public schools in Cleveland Heights through ninth grade, and then entered Windsor Mountain School, Lenox, Massachusetts from which he graduated in 1963. Starting in September 1963 he attended the Massachusetts Institute of Technology, where he obtained an SB degree in Metallurgy in June 1967. During the summers of 1965, '66 and '67 he was employed at the Lewis Research Center of NASA in Cleveland as a summer trainee in the Materials and Stresses Division.

Since September 1967 he has been enrolled as a graduate student in Physical Metallurgy at MIT. During his first two years of graduate study he held the position of Part-time Instructor in the Department of Metallurgy and Materials Science. In June 1969, he received a fellowship sponsored by the Climax Molybdenum Company of Michigan. Following the completion of his studies for the PhD degree he expects to pursue a career of research in private industry.

His interests include music, violin making and playing, art sports, literature, and the pyramids of Egypt.